

# Epitranscriptomic m<sup>6</sup>A Regulation of Axon Regeneration in the Adult Mammalian Nervous System

## Highlights

- PNS nerve injury elevates m<sup>6</sup>A-tagged mRNA encoding RAGs and translational machinery
- PNS nerve injury induces dynamic changes in the m<sup>6</sup>A landscape of adult DRGs
- m<sup>6</sup>A tagging promotes injury-induced global *de novo* protein synthesis in adult DRGs
- m<sup>6</sup>A signaling is required for robust axon regeneration in adult PNS and CNS

## Authors

Yi-Lan Weng, Xu Wang, Ran An, ..., Kai Liu, Hongjun Song, Guo-li Ming

## Correspondence

[gming@pennmedicine.upenn.edu](mailto:gming@pennmedicine.upenn.edu)

## In Brief

N<sup>6</sup>-methyladenosine (m<sup>6</sup>A) occurs in many mRNAs. Weng et al. uncovered an epitranscriptomic mechanism wherein axonal injury elevates m<sup>6</sup>A levels and signaling to promote protein translation, including regeneration-associated genes, which is essential for functional axon regeneration of peripheral sensory neurons.



# Epitranscriptomic m<sup>6</sup>A Regulation of Axon Regeneration in the Adult Mammalian Nervous System

Yi-Lan Weng,<sup>1,2</sup> Xu Wang,<sup>3</sup> Ran An,<sup>1,2,4</sup> Jessica Cassin,<sup>5</sup> Caroline Vissers,<sup>6</sup> Yuanyuan Liu,<sup>7</sup> Yajing Liu,<sup>8</sup> Tianlei Xu,<sup>9</sup> Xinyuan Wang,<sup>1,10</sup> Samuel Zheng Hao Wong,<sup>1,11</sup> Jessica Joseph,<sup>11</sup> Louis C. Dore,<sup>12,13,14</sup> Qiang Dong,<sup>4</sup> Wei Zheng,<sup>15</sup> Peng Jin,<sup>16</sup> Hao Wu,<sup>9</sup> Bin Shen,<sup>7</sup> Xiaoxi Zhuang,<sup>17</sup> Chuan He,<sup>12,13,14</sup> Kai Liu,<sup>3</sup> Hongjun Song,<sup>1,5,6,11,18,19,20</sup> and Guo-li Ming<sup>1,6,11,18,20,21,\*</sup>

<sup>1</sup>Department of Neuroscience, Mahoney Institute for Neurosciences, Perelman School of Medicine, University of Pennsylvania, Philadelphia, PA 19104, USA

<sup>2</sup>Institute for Cell Engineering, Johns Hopkins University School of Medicine, Baltimore, MD 21205, USA

<sup>3</sup>Division of Life Science, State Key Laboratory of Molecular Neuroscience, Hong Kong University of Science and Technology, Hong Kong, China

<sup>4</sup>Department of Neurology, State Key Laboratory of Medical Neurobiology, Huashan Hospital, Fudan University, Shanghai 200040, China

<sup>5</sup>Human Genetic Pre-graduate Program

<sup>6</sup>Biochemistry, Cellular, and Molecular Biology Graduate Program

Johns Hopkins University School of Medicine, Baltimore, MD 21205, USA

<sup>7</sup>State Key Laboratory of Reproductive Medicine, Department of Histology and Embryology, Nanjing Medical University, Nanjing 211166, China

<sup>8</sup>School of Life Science and Technology, ShanghaiTech University, Shanghai 201210, China

<sup>9</sup>Department of Biostatistics and Bioinformatics, Rollins School of Public Health, Emory University, Atlanta, GA 30322, USA

<sup>10</sup>School of Basic Medical Sciences, Fudan University, Shanghai 200040, China

<sup>11</sup>Cellular and Molecular Medicine Graduate Program, Johns Hopkins University School of Medicine, Baltimore, MD 21205, USA

<sup>12</sup>Department of Chemistry

<sup>13</sup>Institute for Biophysical Dynamics

<sup>14</sup>Howard Hughes Medical Institute

University of Chicago, Chicago, IL 60637, USA

<sup>15</sup>National Center for Advancing Translational Sciences, NIH, Bethesda, MD 20892, USA

<sup>16</sup>Department of Human Genetics, School of Medicine, Emory University, Atlanta, GA 30322, USA

<sup>17</sup>Department of Neurobiology, University of Chicago, Chicago, IL 60637, USA

<sup>18</sup>Department of Cell and Developmental Biology

<sup>19</sup>The Epigenetics Institute

<sup>20</sup>Institute for Regenerative Medicine

Perelman School of Medicine, University of Pennsylvania, Philadelphia, PA 19104, USA

<sup>21</sup>Lead Contact

\*Correspondence: [gming@pennmedicine.upenn.edu](mailto:gming@pennmedicine.upenn.edu)

<https://doi.org/10.1016/j.neuron.2017.12.036>

## SUMMARY

N<sup>6</sup>-methyladenosine (m<sup>6</sup>A) affects multiple aspects of mRNA metabolism and regulates developmental transitions by promoting mRNA decay. Little is known about the role of m<sup>6</sup>A in the adult mammalian nervous system. Here we report that sciatic nerve lesion elevates levels of m<sup>6</sup>A-tagged transcripts encoding many regeneration-associated genes and protein translation machinery components in the adult mouse dorsal root ganglion (DRG). Single-base resolution m<sup>6</sup>A-CLIP mapping further reveals a dynamic m<sup>6</sup>A landscape in the adult DRG upon injury. Loss of either m<sup>6</sup>A methyltransferase complex component *Mettl14* or m<sup>6</sup>A-binding protein *Ythdf1* globally attenuates injury-induced protein translation in adult DRGs and reduces functional axon regeneration in the peripheral nervous system *in vivo*. Furthermore, *Pten* deletion-induced axon regenera-

tion of retinal ganglion neurons in the adult central nervous system is attenuated upon *Mettl14* knock-down. Our study reveals a critical epitranscriptomic mechanism in promoting injury-induced protein synthesis and axon regeneration in the adult mammalian nervous system.

## INTRODUCTION

Studies in the past few years have revealed various dynamic modifications of mRNA, including N<sup>6</sup>-methyladenosine (m<sup>6</sup>A), N<sup>1</sup>-methyladenosine (m<sup>1</sup>A), 5-methylcytosine (m<sup>5</sup>C), and pseudouridine ( $\psi$ ) (Gilbert et al., 2016; Li et al., 2016; Zhao et al., 2017a). Among these modifications, m<sup>6</sup>A is the most abundant internal modification of mRNA in eukaryotic cells (Desrosiers et al., 1975). m<sup>6</sup>A sites are present in over 25% of human transcripts, with enrichment in long exons, and near transcription start sites and stop codons (Dominissini et al., 2012; Ke et al., 2015; Meyer et al., 2012). Almost every gene produces both



methylated and unmethylated transcripts, highlighting the highly complex and heterogeneous nature of transcriptomes (Molinie et al., 2016). So far, m<sup>6</sup>A profiling analyses have been performed mostly with cell lines and bulk tissues due to the requirement of a substantial amount of input mRNA (Li et al., 2016). In part due to this technical limitation, the m<sup>6</sup>A landscape and its temporal and spatial dynamics in specific regions of the mammalian nervous system *in vivo* remain largely unknown.

In mammals, m<sup>6</sup>A is installed by a methyltransferase complex consisting of Mettl3, Mettl14, and other components, and can be removed by demethylases Fto and Alkbh5 (Wang et al., 2017; Zhao et al., 2017a). Recent studies have implicated m<sup>6</sup>A in regulating mRNA processing in the nucleus, and translation and decay in the cytoplasm (Zhao et al., 2017a). These different functions of m<sup>6</sup>A modifications are believed to be mediated by diverse m<sup>6</sup>A-binding proteins, such as YT521-B homology domain family (YTHDF) proteins (Zhao et al., 2017a). For example, *in vitro* studies in cell lines have suggested that m<sup>6</sup>A promotes protein translation efficacy via YTHDF1 and YTHDF3, and promotes mRNA decay via YTHDF2 (Li et al., 2017a; Lin et al., 2016; Meyer et al., 2015; Shi et al., 2017; Wang et al., 2015; Zhou et al., 2015). Functionally, m<sup>6</sup>A regulates self-renewal and differentiation of mouse embryonic stem cells and glioblastoma stem cells *in vitro* by promoting mRNA decay (Batista et al., 2014; Cui et al., 2017; Geula et al., 2015; Wang et al., 2014). During development, m<sup>6</sup>A regulates sex determination and neuronal functions by modulating mRNA splicing in *Drosophila* (Hausmann et al., 2016; Lence et al., 2016) and maternal-to-zygotic transition via Ythdf2-mediated maternal mRNA clearance in *Zebrafish* (Zhao et al., 2017b). More recent *in vivo* studies of embryonic mouse development have revealed deficits in stem cell self-renewal and differentiation in the blood and nervous systems (Li et al., 2017b; Yoon et al., 2017; Zhang et al., 2017). These studies have established critical roles for m<sup>6</sup>A-dependent mRNA decay in regulating developmental transitions (Zhao et al., 2017a). The role of m<sup>6</sup>A in the adult mammalian nervous system under physiological and pathological conditions remains largely unexplored.

Sensory neurons in the adult mouse dorsal root ganglion (DRG) exhibit robust axon regeneration in the peripheral nervous system (PNS) through a process involving *de novo* gene transcription and protein synthesis of regeneration-association genes (RAGs) (Costigan et al., 2002; Moore and Goldberg, 2011; Smith and Skene, 1997). Axon regeneration can also be induced in the adult CNS, for example, by *Pten* deletion in retinal ganglion neurons and corticospinal neurons (Liu et al., 2010; Park et al., 2008). Previous studies have identified transcriptional mechanisms that promote intrinsic axon growth capacity (Liu et al., 2011; Moore and Goldberg, 2011; Tedeschi and Bradke, 2017). More recently, epigenetic mechanisms, including both histone acetylation (Cho et al., 2013; Finelli et al., 2013; Gaub et al., 2011; Puttagunta et al., 2014) and DNA methylation (Weng et al., 2017), have been shown to promote transcriptional activation of multiple RAGs, and are required for robust axon regeneration of adult mouse DRG neurons upon peripheral nerve injury (Weng et al., 2013, 2016). The discovery of widespread m<sup>6</sup>A modification and its potential roles in regulating RNA metabolism (Gilbert et al., 2016; Li et al., 2016; Zhao et al., 2017a) raises

the question of whether an epitranscriptomic mechanism may contribute to axon regeneration in the adult mammalian nervous system. Here we investigated the potential role and mechanism of m<sup>6</sup>A methylation in regulating injury responses and axon regeneration in the adult mouse PNS and CNS.

## RESULTS

### Peripheral Axon Injury Elevates m<sup>6</sup>A-Tagged Transcript Levels

Using a mouse line that specifically labels DRG neurons (Kim et al., 2016) and glutamine synthetase as a marker for surrounding satellite glia, we found that m<sup>6</sup>A was present mostly in neurons within the adult DRGs (Figure S1A). Furthermore, peripheral sciatic nerve lesion (SNL) elevated m<sup>6</sup>A levels in adult DRG neurons, reaching a peak around days 1–3 (D1–D3) and then gradually returning back to the basal level (Figures S1A–S1C). We next performed genome-wide profiling of m<sup>6</sup>A-tagged mRNA in the adult DRG under naive and SNL D1 conditions. To overcome limited mRNA input from L4/L5 DRGs of adult mice, we adapted an m<sup>6</sup>A sequencing (m<sup>6</sup>A-seq) method using the SMART2-seq technology, which has recently been used to linearly amplify transcripts for single-cell RNA-seq (Picelli et al., 2014) (named m<sup>6</sup>A-SMART-seq; Figures S1D and S1E). Since the same gene could produce both m<sup>6</sup>A-tagged and untagged transcripts (Molinie et al., 2016), we applied a statistical approach to identify genes for which a substantial proportion of total transcripts was m<sup>6</sup>A tagged (Figure S1F; Table S1). The majority of genes with substantial m<sup>6</sup>A tagging were shared between naive and SNL D1 conditions (Figure 1A). Interestingly, 129 of 304 known RAGs (Chandran et al., 2016) exhibit significant m<sup>6</sup>A tagging at SNL D1 (Figure 1B;  $p < 4.550e-07$ ; hypergeometric test).

We next performed a quantitative comparison of m<sup>6</sup>A-tagged mRNA levels between naive and SNL D1 conditions. A total of 182 m<sup>6</sup>A-tagged genes were substantially upregulated, while few were downregulated (fold change  $\geq 2$ ; Figure 1C; Table S2). Therefore, consistent with m<sup>6</sup>A immunostaining results (Figures S1A–S1C), peripheral nerve injury mostly elevates m<sup>6</sup>A-tagged transcript levels. Notably, 30 RAGs, including *Atf3* (Fagoe et al., 2015; Seiffers et al., 2007), *Sox11* (Jankowski et al., 2009), *Gadd45a* (Befort et al., 2003), and *Tet3* (Weng et al., 2017), exhibited increased levels of m<sup>6</sup>A-tagged transcripts at SNL D1 (Figures 1C and 1D). We validated our m<sup>6</sup>A-SMART-seq results for a select group of RAGs using m<sup>6</sup>A-MerIP qPCR analysis of independent biological samples (Figure 1E; Table S3).

We further performed nonbiased Gene Ontology (GO) analysis for upregulated m<sup>6</sup>A-tagged transcripts. Notably, the most enriched biological term was translation, followed by metabolism-related process (Figure 1F). For example, many transcripts encoding ribosomal subunit proteins, such as *Rps14*, *Rps20*, *Rps23*, *Rps28*, and *Rps29*, and eukaryotic initiation factors, such as *Eif1a* and *Eif3b*, exhibited elevated levels of m<sup>6</sup>A-tagged transcripts at SNL D1 (Figure 1D).

For a given gene, an increase in the m<sup>6</sup>A-tagged transcript level could be due to elevated total transcript levels without changes in the proportion of tagged transcripts, or increased tagging with or without affecting the total transcript level.

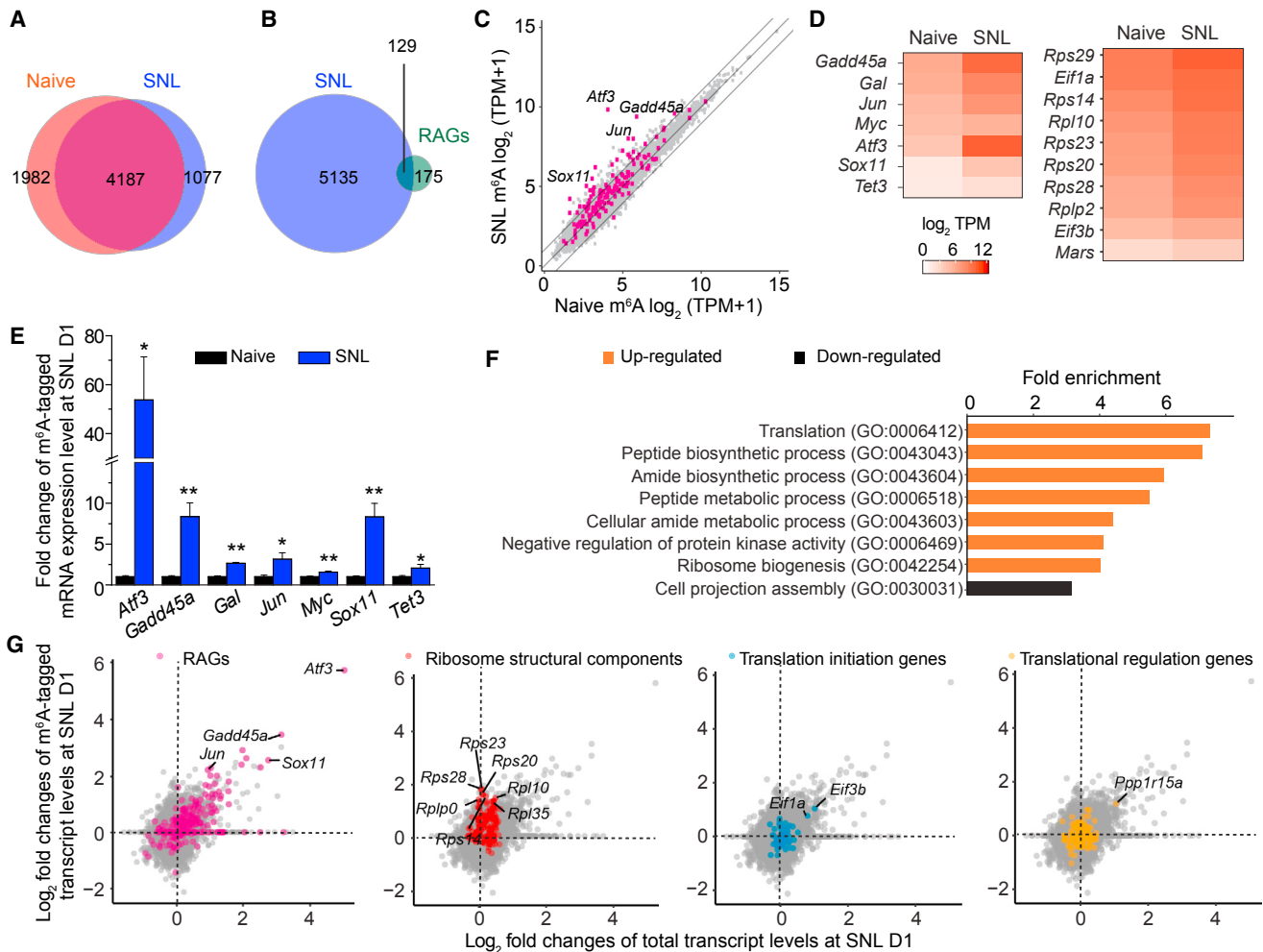


**Figure 1. SNL Upregulates Levels of m<sup>6</sup>A-Tagged mRNAs Encoding RAGs and Protein Translation Machinery in Adult DRGs *In Vivo***

(A) Venn diagram of m<sup>6</sup>A-tagged transcripts identified by m<sup>6</sup>A-SMART-seq in adult mouse DRGs under naive and SNL D1 conditions.

(B) Venn diagram of all m<sup>6</sup>A-tagged genes at SNL D1 and known RAGs.

(C) Scatterplot of expression levels of m<sup>6</sup>A-tagged transcripts under naive and SNL D1 conditions. Lines indicate 2-fold differences and RAGs are indicated by magenta dots.

(D) Heatmap diagrams of the m<sup>6</sup>A transcript levels under naive and SNL D1 conditions for a select group of RAGs and genes related to protein translation functions.

(E) m<sup>6</sup>A-MeRIP qPCR validation of differential m<sup>6</sup>A transcript levels under naive and SNL D1 conditions for selected RAGs. Values are normalized to the naive condition and represent mean  $\pm$  SEM ( $n = 3$  experimental replications from 6 animals; \* $p < 0.05$ ; \*\* $p < 0.01$ ; t test).

(F) GO enrichment analyses of the top 400 genes with increased m<sup>6</sup>A-tagged transcript levels (orange) and the top 400 genes with decreased m<sup>6</sup>A-tagged transcript levels (black) at SNL D1.

(G) Scatterplots of log<sub>2</sub> fold changes of m<sup>6</sup>A-tagged and total transcript levels between naive and SNL D1 conditions. Subsets of genes are labeled with different colors in the same plot: RAGs (magenta), ribosomal subunit-related genes (red), translation initiation-related genes (blue), and translation regulation-related genes (yellow).

See also Figure S1.

Therefore, we compared fold changes in m<sup>6</sup>A-tagged and total transcript levels between naive and SNL D1 conditions. The majority of RAGs, such as *Atf3*, *Sox11*, *Gadd45a*, and *Jun*, exhibited a correlated increase in both m<sup>6</sup>A-tagged and total transcript levels upon SNL, whereas most ribosomal subunit genes with increased m<sup>6</sup>A-tagged transcript levels did not alter their total transcript levels (Figure 1G). Taken together, these quantitative analyses reveal that peripheral nerve injury mostly upregulates m<sup>6</sup>A levels in DRGs with an enrichment of transcripts related to

RAGs and protein translation machinery, involving both transcription activation-coupled m<sup>6</sup>A methylation and an increased proportion of m<sup>6</sup>A-tagged transcript levels without transcription upregulation.

### Single-Base m<sup>6</sup>A Mapping Reveals a Dynamic m<sup>6</sup>A Landscape in Response to Injury

While our m<sup>6</sup>A-SMART-seq approach can quantify the amount of m<sup>6</sup>A-tagged transcripts, it does not identify the location of m<sup>6</sup>A

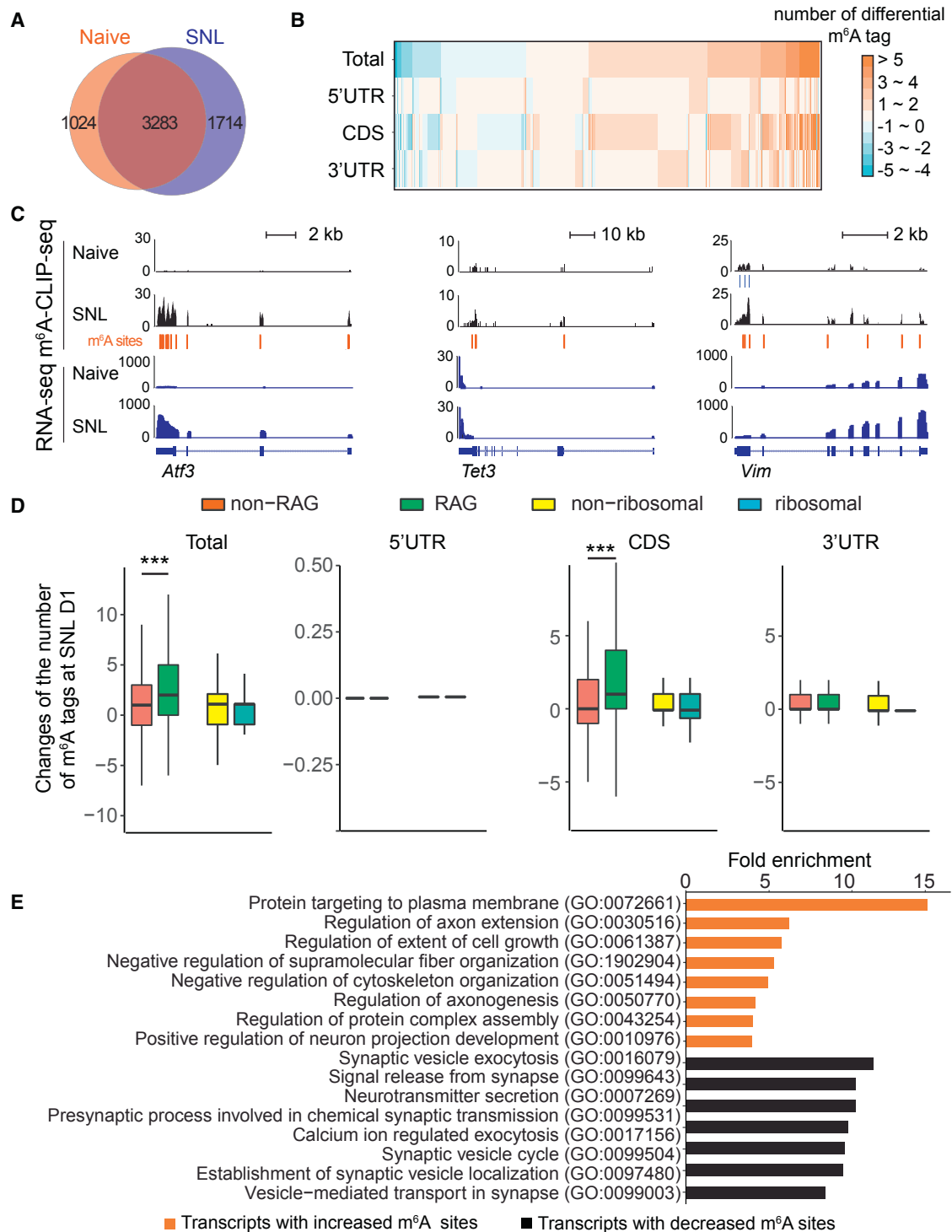


**Figure 2. SNL Modifies the m<sup>6</sup>A Landscape of Transcriptomes of Adult Mouse DRGs In Vivo**

(A) Venn diagram of m<sup>6</sup>A-tagged transcripts identified by m<sup>6</sup>A-CLIP-SMART-seq in adult mouse DRGs under naive and SNL D1 conditions.

(B) Dynamic changes of m<sup>6</sup>A sites in transcripts from adult DRGs at SNL D1. Changes of m<sup>6</sup>A sites are plotted for the whole transcript (total) and in different sub-transcript regions (5' UTR, CDS, and 3' UTR). CDS, coding sequence region.

(C) m<sup>6</sup>A-CLIP-SMART-seq examples for multiple RAGs. Shown are sample tracks for both m<sup>6</sup>A-CLIP-seq (top panels) and RNA-seq (bottom panels). CLIP unique tag coverage is shown in black, and m<sup>6</sup>A sites are indicated with vertical lines.

(legend continued on next page)

sites within transcripts. We next performed m<sup>6</sup>A-CLIP-seq, which provides single-base resolution mapping of m<sup>6</sup>A across the transcriptome (Linder et al., 2015). Similarly, we adapted the SMART2-seq technology to overcome the small amount of mRNA input from L4/L5 DRGs (named m<sup>6</sup>A-CLIP-SMART-seq; Figures S2A and S2B; Table S4). Under both naive and SNL D1 conditions, we identified m<sup>6</sup>A sites enriched in exons and near transcription start sites and stop codons across transcriptomes (Figures S2C and S2D), which is similar to previous findings from cell lines (Linder et al., 2015).

Consistent with our m<sup>6</sup>A-SMART-seq results (Figure 1A), m<sup>6</sup>A-CLIP-SMART-seq showed that the majority of m<sup>6</sup>A-tagged transcripts was shared between naive and SNL D1 conditions (Figure 2A). Notably, there were dynamic changes in m<sup>6</sup>A sites (Figure 2B). Some transcripts exhibited a gain and/or loss of m<sup>6</sup>A sites across the 5' UTR, coding regions, and 3' UTR, whereas other transcripts displayed region-specific changes (Figure 2B; Table S5). Multiple RAGs, such as *Atf3* and *Tet3*, gained new m<sup>6</sup>A sites upon SNL (Figure 2C). Notably, transcripts encoding retrograde injury signaling molecules, such as Vimentin (*Vim*) (Perlson et al., 2005), exhibited dynamic m<sup>6</sup>A sites upon SNL (Figure 2C). In general, RAG transcripts exhibited a larger gain in m<sup>6</sup>A sites compared to non-RAG transcripts and new sites were located mostly in coding regions, whereas ribosomal subunit-related genes exhibited a similar gain in m<sup>6</sup>A sites as other genes (Figure 2D). Across the transcriptome, GO analysis showed that transcripts with newly added m<sup>6</sup>A sites were enriched for axonal regulation, whereas transcripts with a loss of m<sup>6</sup>A sites were enriched for presynaptic functions of neurons (Figure 2E).

We next cross-compared m<sup>6</sup>A-seq and m<sup>6</sup>A-CLIP-seq datasets. While many RAGs exhibited increased m<sup>6</sup>A-tagged transcripts and gained new m<sup>6</sup>A sites, most transcripts encoding protein translation machinery components showed increased m<sup>6</sup>A-tagged transcript levels, but not new m<sup>6</sup>A sites (Figure S2E). Together, our quantitative and single-base m<sup>6</sup>A mapping reveals a dynamic landscape of mRNA methylation in adult DRGs in response to injury.

### Mettl14 Regulates Injury-Induced De Novo Protein Synthesis

To determine the function of m<sup>6</sup>A in the adult DRG, we examined conditional knockout mice of *Mettl14* (Yoon et al., 2017), a core subunit of the mammalian m<sup>6</sup>A methyltransferase complex (Wang et al., 2017). We deleted *Mettl14* specifically in post-mitotic neurons *in vivo* using the *Syn1-Cre;Mettl14<sup>fl/fl</sup>* (cKO) model. We confirmed *Mettl14* deletion in adult DRGs at the protein level by western blot (Figure S3A). Quantitative dot blot analysis showed largely diminished m<sup>6</sup>A levels in purified mRNA from cKO DRGs compared to wild-type (WT) littermates (Figure 3A).

m<sup>6</sup>A methylation has been implicated in regulating both mRNA decay and protein translation of tagged transcripts (Zhao et al., 2017a). To examine the potential impact of m<sup>6</sup>A on total mRNA levels, we performed RNA-seq analysis of adult DRGs from WT and *Mettl14* cKO mice under both naive and SNL D1 conditions (Table S6). We found very similar gene expression profiles between WT and cKO DRGs, under both naive and injury conditions (Figure S3B). For RAGs, we also observed similar induction in WT and cKO DRGs (Figure 3B). Therefore, the impact of m<sup>6</sup>A methylation on total transcript levels appears to be minimal under our experimental conditions.

We next examined the effect of *Mettl14* deletion on protein translation in the adult DRG. We employed the SUNSET assay *in vivo* to label nascent proteins with puromycin (Goodman et al., 2011; Schmidt et al., 2009) (Figure S3C). Analysis of WT adult DRGs showed a global increase of new protein synthesis at SNL D1 (Figures 3C, 3D, and S3D), indicating that peripheral nerve lesion promotes protein translation in the cell body as part of the injury response. In *Mettl14* cKO DRGs, SNL-induced protein synthesis was significantly reduced globally compared to WT DRGs, whereas the basal level under the naive condition was similar to WT (Figures 3C, 3D, and S3D). To validate our result using an independent approach, we examined *Atf3*, one of the most robustly induced genes by SNL, which has been shown to enhance peripheral nerve regeneration by increasing the intrinsic growth competence of adult DRG neurons (Fagoie et al., 2015; Seiffers et al., 2007). The *Atf3* mRNA was also induced in *Mettl14* cKO DRGs, although at a lower level compared to WT at SNL D1 (Figure S3E). We confirmed the loss of m<sup>6</sup>A methylation in *Atf3* mRNA in *Mettl14* cKO DRGs (Figure S3F). Immunostaining showed little ATF3 protein expression under the naive condition, in contrast to robust induction at SNL D1 in WT adult DRGs (Figures 3E and 3F). This induction was drastically reduced in *Mettl14* cKO DRGs at SNL D1 (Figures 3E and 3F). Using quantitative western blot analysis, further time course analysis showed a delayed induction of ATF3 protein in *Mettl14* cKO DRGs (Figures 3G and 3H). Together, these results indicate that *Mettl14*-mediated m<sup>6</sup>A methylation is critical for SNL-induced protein translation in adult DRGs *in vivo*, which is known to promote axon regeneration of mature mammalian neurons (Abe et al., 2010).

### Mettl14 Is Required for Robust DRG Neuron Axon Regeneration and Behavioral Recovery

We next directly examined the functional role of *Mettl14* on axon regeneration of DRG neurons after injury. We first used an *in vitro* neurite outgrowth assay with primary neurons from adult mouse DRGs (Chen et al., 2017). Cultures were infected with AAV2 to express the short hairpin RNA (shRNA) against *Mettl14* (Wang et al., 2014), followed by re-plating to mimic axotomy. We found that expression of shRNA-*Mettl14* reduced the length of the

(D) Comparison of dynamic m<sup>6</sup>A sites between RAGs and non-RAGs, and between transcripts encoding ribosomal subunit-related and non-ribosomal subunit-related proteins, in different transcript regions (total, 5' UTR, CDS, and 3' UTR) under naive and SNL D1 conditions. Values represent mean differential m<sup>6</sup>A tag numbers (n = 154 RAGs and 5,867 non-RAGs; n = 55 ribosomal subunit-related and 5,966 non-ribosomal subunit-related genes; \*\*\*p < 0.001; one-way ANOVA with Tukey's post hoc test).

(E) GO enrichment analyses of transcripts with differential m<sup>6</sup>A sites at SNL D1. See also Figure S2.

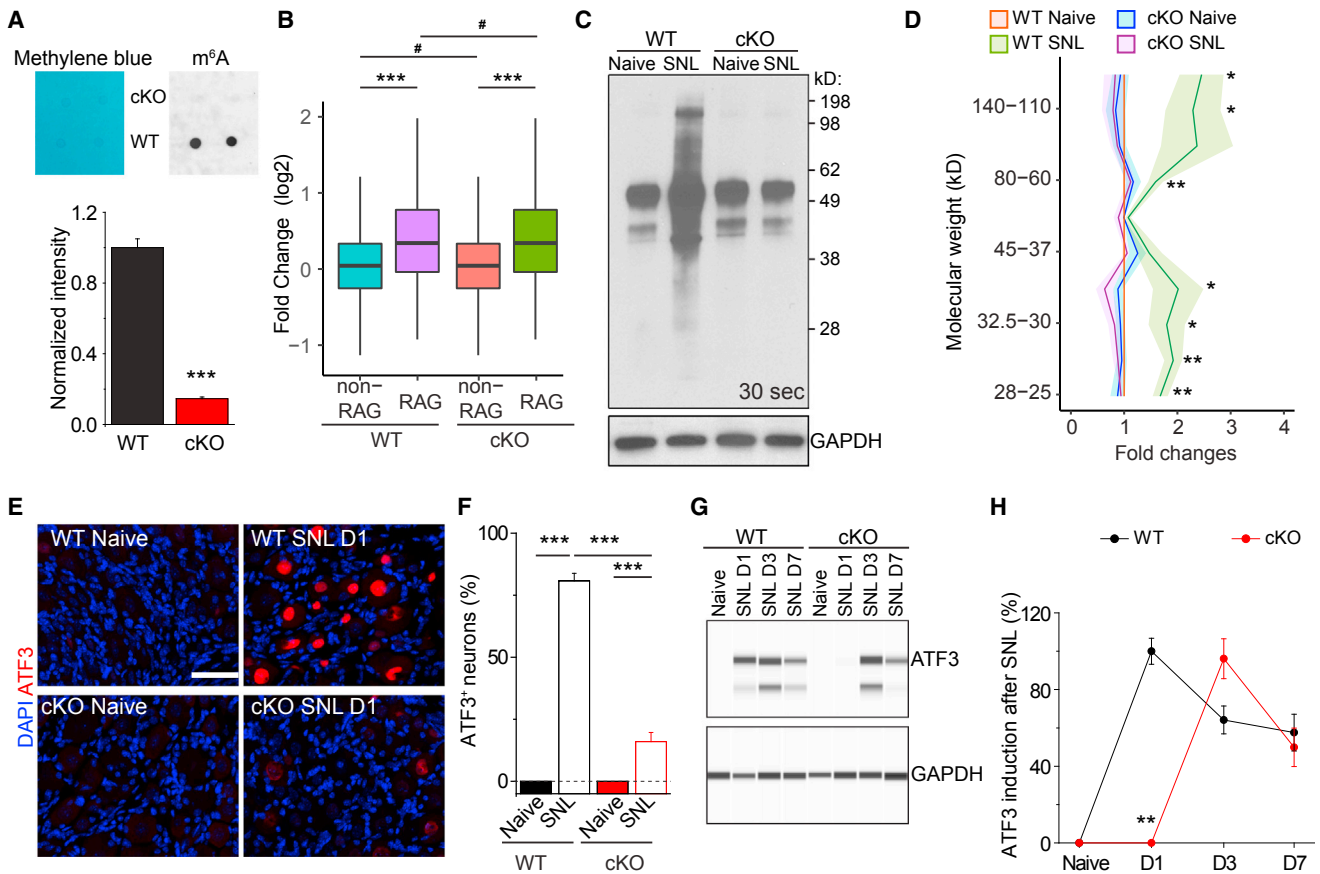


**Figure 3. *Mettl14* Deletion Attenuates SNL-Induced Global Protein Translation and ATF3 Protein Expression in the Adult DRG**

(A)  $m^6A$  dot blot showing diminished  $m^6A$  levels in mRNA from DRGs of adult *Syn-Cre;Mettl14* cKO mice. Methylene blue was used to assess the equal loading of mRNA. Representative images (top panel) and quantification (bottom panel) are shown. Values represent mean  $\pm$  SEM ( $n = 2$  animals per group; \*\*\* $p < 0.001$ ; two-way ANOVA).

(B) Boxplots depicting the fold changes of the gene expression level between RAGs and non-RAGs after injury in WT and *Mettl14* cKO DRGs. Each box shows the first quartile, median, and third quartile (\*\*\* $p < 0.001$ ; # $p > 0.05$ ; one-way ANOVA with Tukey's post hoc test).

(C and D) SUnSET analysis of new protein synthesis in adult L4/5 DRGs of WT and *Mettl14* cKO mice. *De novo* synthesized proteins were pulse-chase labeled for 1 hr after injection of puromycin at SNL D1. Western blot of DRG lysates was performed for different conditions. GAPDH was used as the loading control. Representative images (C) and quantification (D) are shown. Values are normalized to the WT naive condition and plots represent ranges of mean  $\pm$  SEM ( $n = 4$  animals; \*\* $p < 0.01$ ; \* $p < 0.05$ ; two-way ANOVA). See Figure S3E for images from different exposures of the same western blot example.

(E and F) Assessment of ATF3 induction in WT and *Mettl14* cKO DRGs at SNL D1. Sample images of ATF3 immunostaining (E) and quantification (F) are shown. Scale bars, 50  $\mu$ m. Values represent mean  $\pm$  SEM ( $n = 4$  animals; \*\*\* $p < 0.001$ ; two-way ANOVA).

(G and H) Time course analysis of ATF3 induction in WT and *Mettl14* cKO adult DRGs. Immunoassay of DRG protein lysates was performed by capillary electrophoresis. GAPDH was used as the loading control. Sample images of blots (G) and quantification (H) are shown. Values represent mean  $\pm$  SEM ( $n = 3$  animals; \*\* $p < 0.01$ ; two-way ANOVA).

See also Figure S3.

longest neuronal process of each neuron compared to expression of shRNA-control, indicating an important role of *Mettl14* in axon regeneration of DRG neurons (Figures S4A and S4B).

We next assessed the *in vivo* role of *Mettl14* in functional axon regeneration of adult DRG neurons after SNL. To avoid potential complications of *Mettl14* deletion on DRG neuronal development and maturation in the *Syn1-Cre;Mettl14<sup>fl/fl</sup>* cKO model, we instead infected L4/L5 DRGs in adult *Mettl14<sup>fl/fl</sup>* mice via targeted intrathecal injection of AAV2/9 expressing Cre (Weng et al., 2017). This approach leads to infection of over 70% of all neurons, but not surrounding satellite glia, in L4/5 DRGs (Figure S4C) (Weng et al., 2017). Regenerating sensory axons were identified

by SCG10 immunostaining at SNL D3 (Shin et al., 2014). We found that extension of SCG10<sup>+</sup> axons was substantially decreased in AAV-Cre;*Mettl14* cKO mice compared to WT littermates (Figures 4A and 4B). Similar results were obtained from the *Syn1-Cre;Mettl14<sup>fl/fl</sup>* cKO model (Figures S4D and S4E). We observed minimal cleaved-caspase 3 expression in the adult DRG upon SNL, indicating that cell death is not a major factor under these conditions (Figure S4F).

Regenerating axons of sciatic nerves extend to the epidermis and start to re-innervate the skin of the hindpaw around 2–3 weeks after injury (Weng et al., 2017). Analysis of skin biopsies showed no PGP9.5<sup>+</sup> sensory axon innervation to the

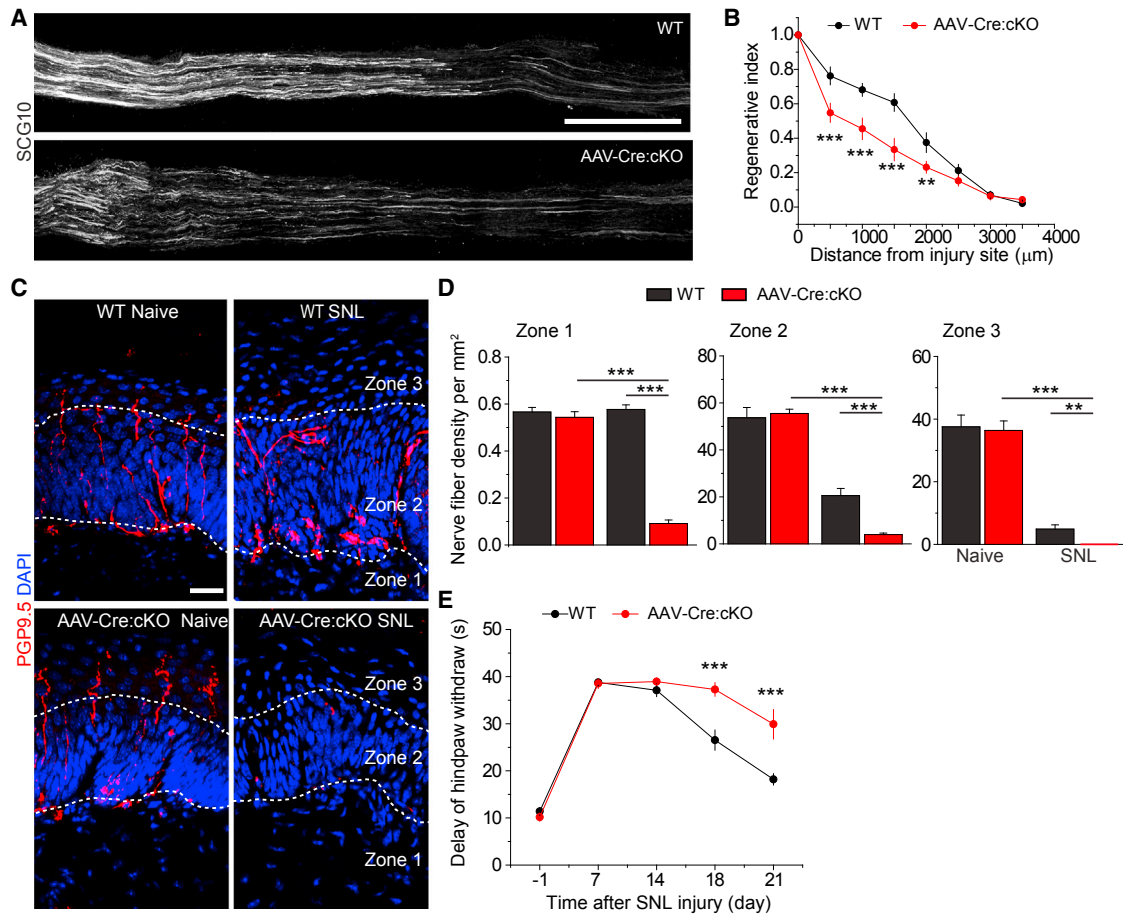


#### Figure 4. *Mettl14* Deletion Attenuates Functional Axon Regeneration of Adult DRG Neurons *In Vivo*

(A and B) Analysis of regeneration of sensory axons by SCG10 immunostaining at SNL D3 in adult WT and *Mettl14*<sup>fl/fl</sup> mice upon intrathecal injection of AAV2/9 to express Cre. Sample images of regenerating sensory axons identified by SCG10 (A; scale bar, 1 mm) and quantification (B) are shown. SCG10 immunofluorescence intensity was measured at different distal distances and normalized to that at 1 mm before the lesion site as the regenerative index. Values represent mean  $\pm$  SEM (n = 8 animals for WT and 10 animals for AAV-Cre;*Mettl14* cKO; \*\*\*p < 0.001; \*\*p < 0.01; two-way ANOVA).

(C and D) Assay for re-innervation of the hindpaw epidermal area by regenerating sensory axons. Sample images of cross-sections of hindpaw glabrous skin of WT and AAV-Cre;*Mettl14* cKO mice immunostained with the pan-neuronal marker PGP9.5 are shown (C). The dotted line indicates the border between dermis and epidermis. Scale bar, 20  $\mu$ m. Also shown are quantifications of the number of intra-epidermal nerve fibers in a 1 mm segment of different epidermal areas (D). Values represent mean  $\pm$  SEM (n = 5 animals per group; \*\*\*p < 0.001; \*\*p < 0.01; two-way ANOVA).

(E) Assessment of thermal sensory recovery after SNL in WT and AAV-Cre;*Mettl14* cKO mice. Values represent mean  $\pm$  SEM (n = 10 animals per group; \*\*\*p < 0.001; two-way ANOVA).

See also Figure S4.

epidermis of the hindpaw at SNL D7, indicating effective degeneration of pre-existing mature axons of both WT and AAV-Cre;*Mettl14* cKO DRG neurons (Figure S4G). At SNL D21, innervation to all three epidermal zones by regenerating axons in adult AAV-Cre;*Mettl14* cKO mice was significantly reduced compared to those in WT mice, but no difference was observed under the naive condition (Figures 4C and 4D).

To further assess the functional outcome on axon regeneration, we performed a behavioral test to quantify the latency of heat-evoked hindpaw withdrawal (Wright et al., 2014). Both WT and AAV-Cre;*Mettl14* cKO animals exhibited similar response latencies to a radiant thermal stimulus at SNL D1 and D7 (Figure 4E). Starting from SNL D18, the withdrawal latency gradually recovered in the WT group, but only minimally

recovered in *Mettl14* cKO animals (Figure 4E). Together, these results indicate an essential role of m<sup>6</sup>A mRNA methylation in functional sensory axon regeneration of adult DRG neurons *in vivo*.

#### YTHDF1 Is Required for SNL-Induced Global Protein Synthesis and Robust Axon Regeneration of DRG Neurons

To further support our model that m<sup>6</sup>A signaling promotes global protein synthesis and axon regeneration upon injury and to investigate the downstream mechanism, we examined the KO mice of *Ythdf1* (Figure S5A), an m<sup>6</sup>A reader that has been implicated in promoting protein translation efficacy of m<sup>6</sup>A-tagged transcripts in cell lines (Shi et al., 2017; Wang et al., 2015).

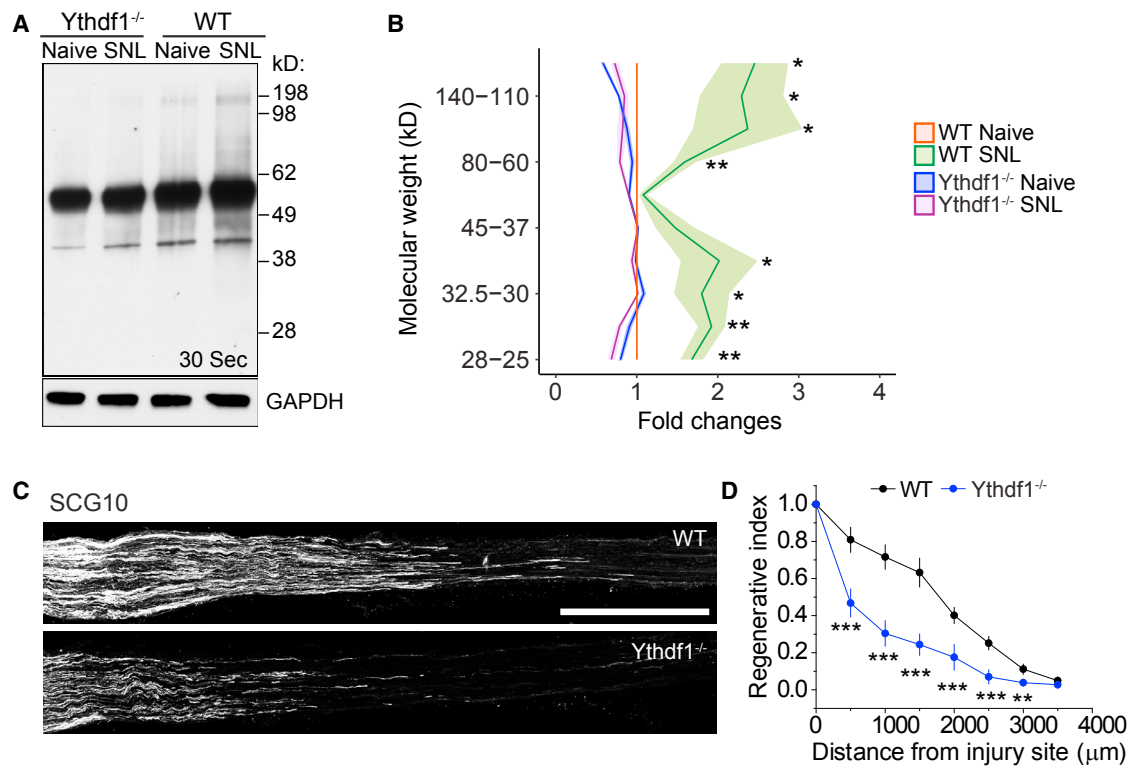


**Figure 5. YTHDF1 Is Required for Injury-Induced Global *De Novo* Protein Synthesis and Robust Axon Regeneration of Adult DRG Neurons**

(A and B) SUNSET analysis of new protein synthesis in adult L4/5 DRGs of WT and *Ythdf1* KO mice. *De novo* synthesized proteins were pulse-chase labeled for 1 hr after injection of puromycin at SNL D1. Western blot of DRG lysates was performed for different conditions. GAPDH was used as the loading control. Representative images (A) and quantification (B) are shown. Values are normalized to WT naive conditions and plots represent ranges of mean  $\pm$  SEM ( $n = 3$  for WT and *Ythdf1* KO; \*\*\* $p < 0.01$ ; \*\* $p < 0.01$ ; two-way ANOVA). See Figure S5C for images from different exposures of the same western blot example.

(C and D) Analysis of regeneration of sensory axons by SCG10 immunostaining at SNL D3 in adult WT and *Ythdf1* KO mice. Sample images of regenerating sensory axons identified by SCG10 (C; scale bar, 1 mm) and quantification (D) are shown. SCG10 immunofluorescence intensity was measured at different distal distances and normalized to the level 1 mm before the lesion site as the regenerative index. Values represent mean  $\pm$  SEM ( $n = 7$  animals for WT and 6 animals for *Ythdf1* KO mice; \*\*\* $p < 0.001$ ; \*\* $p < 0.01$ ; two-way ANOVA).

See also Figure S5.

qPCR analysis showed similar induction of RAGs at mRNA levels in WT and *Ythdf1* KO adult DRGs (Figure S5B). In contrast, the SUNSET assay revealed a marked reduction of SNL-induced global *de novo* protein synthesis in adult DRGs of *Ythdf1* KO mice (Figures 5A, 5B, and S5C). Similar to *Mettl14* deletion, the extension of regenerating SCG10<sup>+</sup> axons was substantially reduced in *Ythdf1* KO mice compared to WT mice at SNL D3 (Figures 5C and 5D). We observed minimal cleaved-caspase 3 expression in the adult DRG in WT and *Ythdf1* cKO mice upon SNL (Figure S5D). Together, these results further support our model and identify YTHDF1 as a key player in promoting injury-induced protein translation and axon regeneration of adult DRGs *in vivo*.

#### **Mettl14 Is Required for *Pten* Deletion-Induced Robust Axon Regeneration of Adult Retinal Ganglion Neurons**

Finally, we assessed whether m<sup>6</sup>A signaling is also involved in axon regeneration in the adult CNS. We employed the model of *Pten* deletion-induced axon regeneration of retinal ganglion cells (RGCs) in adult mice (Park et al., 2008). We co-expressed Cre and

shRNA-Mettl14 in adult RGCs by AAV, followed by axotomy, axonal labeling, and analysis in *Pten* cKO or WT mice (Park et al., 2008). Expression of shRNA-Mettl14 alone did not lead to any axon regeneration of RGCs (Figure S6A), but markedly attenuated *Pten* deletion-induced regeneration compared to shRNA-control (Figures 6A and 6B). The ratio of phospho-S6<sup>+</sup> RGCs remained the same between expression of shRNA-control and shRNA-Mettl14 in *Pten* cKO mice (Figures 6C and 6D), suggesting that blockage of axon regeneration is not likely to be due to the inactivation of mTOR signaling. Notably, there was a 35.1% reduction in the number of Tuj1<sup>+</sup> RGCs upon *Mettl14* knockdown in the *Pten* cKO mice, but not in the WT mice (Figures 6D, S6B, and S6C), suggesting that *Mettl14* is also involved in *Pten* deletion-induced survival of RGCs. There was a larger decrease in the number of regenerating axons at all distances examined (53.3% reduction on average; Figure 6B), indicating that the survival effect alone could not explain the impact of *Mettl14* knockdown on axon regeneration in *Pten* cKO mice. Previous studies have shown that survival rates varied dramatically among neuronal subtypes in the adult retina, with SMI32<sup>+</sup> alpha-RGCs

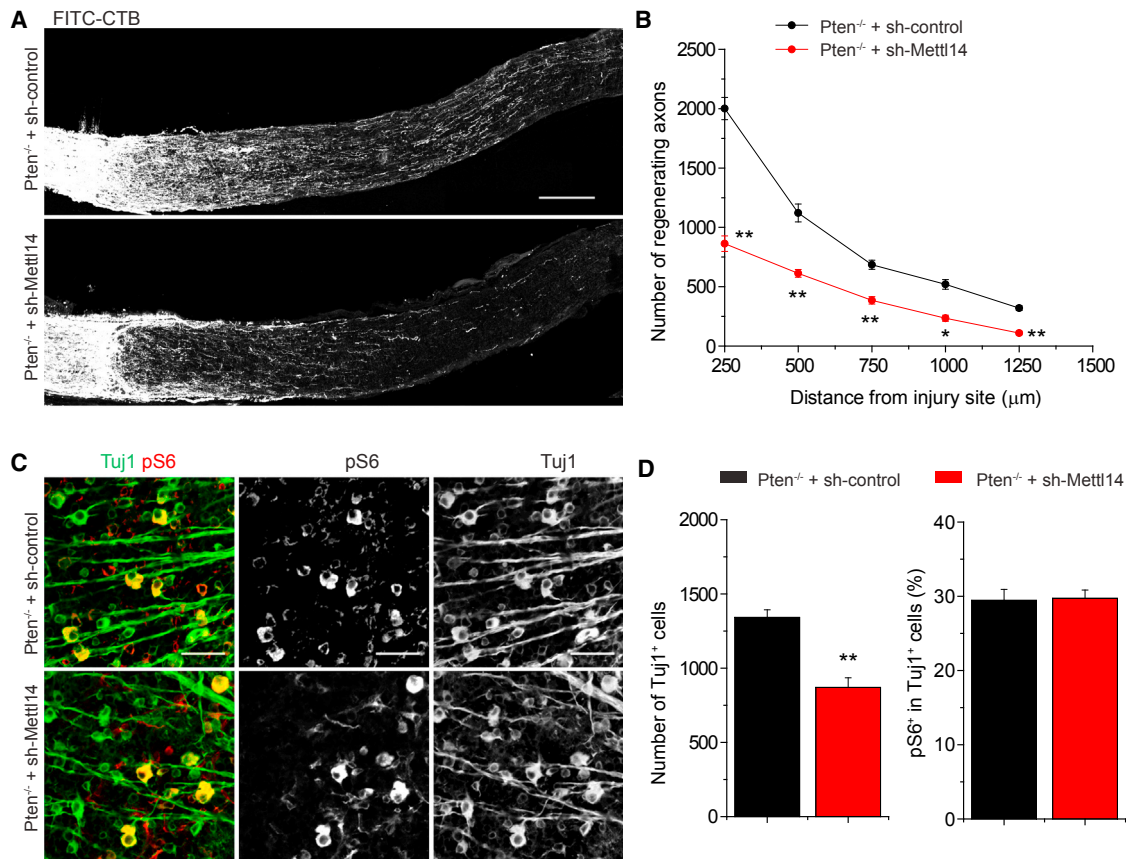


**Figure 6. Mettl14 Is Required for Robust *Pten* Deletion-Induced Axonal Regeneration of Retinal Ganglion Neurons in the Adult Mouse CNS** Adult *Pten*<sup>fl/fl</sup> mice were co-injected with AAV-Cre and AAV-shRNA-control or AAV-shRNA-Mettl14. Optic nerve was crushed 4 weeks after AAV injection and RGC axons were traced by fluorescence conjugated cholera toxin B (FITC-CTB) 2 weeks later. Shown are sample images of sections of optic nerve containing FITC-CTB-labeled axons (A; scale bar, 200 μm) and quantification of numbers of regenerating axons at different distances from the injury site (B). Values represent mean ± SEM (n = 5 animals per group; \*\*p < 0.01; \*p < 0.05; ANOVA followed by Fisher's least significant difference). Also shown are sample images of whole-mount retina with TuJ1 (green) and pS6 (red) immunostaining (C; scale bar, 50 μm) and quantification of densities of TuJ1<sup>+</sup> RGCs and percentages of TuJ1<sup>+</sup> RGCs expressing pS6 (D). Values represent mean ± SEM (n = 5 animals per each group; \*\*p < 0.01; Student's t test). See also Figure S6.

(αRGCs) surviving preferentially and accounting for nearly all axon regeneration following *Pten* deletion (Duan et al., 2015). We found that the percentage of αRGCs among surviving TuJ1<sup>+</sup> RGCs was not affected by *Mettl14* knockdown in *Pten* cKO mice (Figure S6D). Together, these results suggest that *Mettl14* promotes both survival and axonal extension of *Pten*<sup>-/-</sup> RGCs after injury in the adult CNS.

## DISCUSSION

Our study reveals a critical role of m<sup>6</sup>A epitranscriptomic regulation in injury responses and functional axon regeneration in the adult mammalian nervous system *in vivo*. *De novo* gene transcription and protein translation are known to be required for robust axon regeneration of adult neurons upon injury and previous studies have identified important roles of transcriptional and epigenetic mechanisms, including both histone and DNA modifications (Cho and Cavalli, 2014; Trakhtenberg and Goldberg, 2012; Weng et al., 2016; Wong and Zou, 2014). Our study reveals

another layer of regulation and suggests a model wherein PNS injury elevates methylated mRNA transcripts, including RAGs, which are then subjected to enhanced protein translation for effective axon regeneration. The finding that some epigenetic regulators, such as *Tet3* and *Gadd45* a (Guo et al., 2011; Yao et al., 2016), are m<sup>6</sup>A tagged suggests a potential interaction between epigenetic and epitranscriptomic pathways. Our initial study also suggests a similar role of m<sup>6</sup>A epitranscriptomic regulation of induced axon regeneration in the adult mammalian CNS.

Mechanistically, our study provides *in vivo* evidence for a critical role of m<sup>6</sup>A in promoting protein translation in the mammalian system. Different from previous findings on the *in vivo* role of m<sup>6</sup>A-dependent promotion of mRNA decay in regulating embryonic development (Li et al., 2017b; Yoon et al., 2017; Zhang et al., 2017; Zhao et al., 2017b), the impact of m<sup>6</sup>A methylation on total mRNA levels appears to be minimal in adult mouse DRGs under both basal and injury conditions. Instead, m<sup>6</sup>A plays a critical role in peripheral nerve

injury-induced global protein translation in adult mouse DRGs *in vivo* via YTHDF1. *De novo* protein synthesis is known to be critical for axon regeneration in the adult mammalian PNS and CNS (Belin et al., 2015; Cho et al., 2015; Donnelly et al., 2013; Jung et al., 2012; Rishal and Fainzilber, 2014; Song and Poo, 2001; van Niekerk et al., 2016). We have identified three classes of transcripts with substantial m<sup>6</sup>A tagging. First, many transcripts encoding RAGs exhibit elevated m<sup>6</sup>A levels and new m<sup>6</sup>A sites upon SNL. Second, some retrograde injury signaling molecules exhibit m<sup>6</sup>A tagging and increased m<sup>6</sup>A sites upon SNL. This result raises the possibility that m<sup>6</sup>A tagging may promote local protein translation to enhance retrograde signaling upon injury, which is known to be required for robust axonal regeneration of DRG neurons (Rishal and Fainzilber, 2014). Third, many transcripts encoding the molecular machinery for protein translation, including both ribosomal subunits and initial complex components, are themselves m<sup>6</sup>A tagged. Therefore, injury may promote global protein translation by augmenting the general translation machinery. Together, this injury-induced reconfiguration of the epitranscriptome may prioritize mechanisms to synthesize critical factors and rapidly turn on the regenerative program. How the specificity of dynamic m<sup>6</sup>A modification arises is an important question for future investigation. Our detailed analysis of ATF3 in *Mett14* cKO mice showed a delayed induction at the protein level (Figures 3G and 3H), yet functional axon regeneration did not recover (Figure 4E). It is likely that injury induces a coordinated response with a cascade of *de novo* gene expression and protein synthesis. We thus propose a model wherein m<sup>6</sup>A methylation is critical for the coordination of new protein synthesis in injury responses, deficits of which lead to defective axon regeneration and functional recovery.

Typically, MeRIP-seq and HITS-CLIP-seq have been used for m<sup>6</sup>A or protein-RNA interaction profiling. One major technical limitation of these methods is that the library preparation normally requires a large amount of starting material and the process involves multiple tedious steps. To overcome limitations imposed on the quantity of source material imposed by the small number of axotomized DRGs, we developed new methods for library construction to quantify m<sup>6</sup>A-tagged transcript levels and identify m<sup>6</sup>A locations. Our approach not only utilizes a template-switching mechanism to avoid effects of ligation bias, but also substantially increases the sensitivity and shortens the processing time. These techniques will allow analyses of epitranscriptomes, including m<sup>6</sup>A, m<sup>1</sup>A, and potentially other mRNA modifications, in a tissue-specific manner.

m<sup>6</sup>A levels increase over development in the mouse nervous system (Meyer et al., 2012) and can be dynamically regulated via active demethylation (Jia et al., 2011; Zheng et al., 2013). Recent studies of the m<sup>6</sup>A demethylase Fto have revealed its critical roles in regulating adult neurogenesis (Li et al., 2017c), memory formation and consolidation (Walters et al., 2017; Widagdo et al., 2016), and local axonal protein translation (Yu et al., 2017). Together with these studies, our findings suggest that m<sup>6</sup>A mRNA methylation may play a broader role in normal physiology and responses to pathological stimuli in the adult mammalian nervous system.

## STAR★METHODS

Detailed methods are provided in the online version of this paper and include the following:

- KEY RESOURCES TABLE
- CONTACT FOR REAGENT AND RESOURCE SHARING
- EXPERIMENTAL MODEL AND SUBJECT DETAILS
  - Animals
- METHOD DETAILS
  - AAV constructs
  - Animal surgery
  - DRG cultures and neurite outgrowth assay
  - m<sup>6</sup>A-SMART-seq
  - m<sup>6</sup>A-CLIP-SMART-seq
  - RNA-seq
  - Analysis m<sup>6</sup>A-SMART-Seq and RNA-seq
  - Analysis of m<sup>6</sup>A-CLIP-SMART-seq
  - m<sup>6</sup>A-MeRIP Q-PCR
  - m<sup>6</sup>A dot blot analysis
  - Immunohistology, imaging and analysis
  - Measurement of newly synthesized protein
  - Capillary electrophoresis immunoassay
  - Western blot analysis
  - *In vivo* DRG axon regeneration assay
  - Behavioral analysis
  - Optic nerve regeneration quantifications
- QUANTIFICATION AND STATISTICAL ANALYSIS
- DATA AND SOFTWARE AVAILABILITY

## SUPPLEMENTAL INFORMATION

Supplemental Information includes six figures and six tables and can be found with this article online at <https://doi.org/10.1016/j.neuron.2017.12.036>.

## ACKNOWLEDGMENTS

We thank members of Ming and Song laboratories and the Dr. Miriam and Sheldon G. Adelson Medical Research Foundation (AMRF) investigators for discussion; J. Schnoll and K. Christian for comments; and Y. Cai, L. Liu, and D. Johnson for technical support. This work was supported by grants from AMRF (to G.-I.M.), NIH (P01NS097206 and RM1HG008935 to H.S., P.J., and C.H.; R37NS047344 to H.S.; and R35NS097370 to G.-I.M.), Hong Kong Research Grants Council (16103315 and 16149316 to K.L.), and National Natural Science Foundation of China (81671214 to K.L.). C.H. is an HHMI investigator.

## AUTHOR CONTRIBUTIONS

Y.-L.W. led the project and was involved in all aspects of the study. Xu Wang and K.L. performed *in vitro* neurite outgrowth of DRG neurons and optic nerve injury studies. R.A. performed surgical procedures and data quantification for DRG studies. T.X., P.J., and H.W. helped with some of the bioinformatics analyses, and J.C., C.V., Xinyuan Wang, S.Z.H.W., J.J., Q.D., and W.Z. contributed to other data collection. L.C.D., X.Z., and C.H. provided *Mett14*<sup>fl/fl</sup> mice. Yuanyuan Liu, Yajing Liu, B.S., X.Z., and C.H. provided *Ythdf1*<sup>-/-</sup> mice. Y.-L.W., H.S., and G.-I.M. designed the project, analyzed the data, and wrote the paper. All authors helped prepare the manuscript.

## DECLARATION OF INTERESTS

The authors declare no competing interests.

Received: June 23, 2017  
 Revised: November 5, 2017  
 Accepted: December 22, 2017  
 Published: January 17, 2018

## REFERENCES

- Abe, N., Borson, S.H., Gambello, M.J., Wang, F., and Cavalli, V. (2010). Mammalian target of rapamycin (mTOR) activation increases axonal growth capacity of injured peripheral nerves. *J. Biol. Chem.* **285**, 28034–28043.
- Batista, P.J., Molinie, B., Wang, J., Qu, K., Zhang, J., Li, L., Bouley, D.M., Lujan, E., Haddad, B., Daneshvar, K., et al. (2014). m(6)A RNA modification controls cell fate transition in mammalian embryonic stem cells. *Cell Stem Cell* **15**, 707–719.
- Befort, K., Karchewski, L., Lanoue, C., and Woolf, C.J. (2003). Selective up-regulation of the growth arrest DNA damage-inducible gene Gadd45 alpha in sensory and motor neurons after peripheral nerve injury. *Eur. J. Neurosci.* **18**, 911–922.
- Belin, S., Nawabi, H., Wang, C., Tang, S., Latremoliere, A., Warren, P., Schorle, H., Uncu, C., Woolf, C.J., He, Z., and Steen, J.A. (2015). Injury-induced decline of intrinsic regenerative ability revealed by quantitative proteomics. *Neuron* **86**, 1000–1014.
- Bolger, A.M., Lohse, M., and Usadel, B. (2014). Trimmomatic: a flexible trimmer for Illumina sequence data. *Bioinformatics* **30**, 2114–2120.
- Bonaguidi, M.A., Wheeler, M.A., Shapiro, J.S., Stadel, R.P., Sun, G.J., Ming, G.L., and Song, H. (2011). In vivo clonal analysis reveals self-renewing and multipotent adult neural stem cell characteristics. *Cell* **145**, 1142–1155.
- Chandran, V., Coppola, G., Nawabi, H., Omura, T., Versano, R., Huebner, E.A., Zhang, A., Costigan, M., Yekkiral, A., Barrett, L., et al. (2016). A systems-level analysis of the peripheral nerve intrinsic axonal growth program. *Neuron* **89**, 956–970.
- Chen, W., Lu, N., Ding, Y., Wang, Y., Chan, L.T., Wang, X., Gao, X., Jiang, S., and Liu, K. (2017). Rapamycin-resistant mTOR activity is required for sensory axon regeneration induced by a conditioning lesion. *eNeuro* **3**, ENEURO.0358-16.2016.
- Cho, Y., and Cavalli, V. (2014). HDAC signaling in neuronal development and axon regeneration. *Curr. Opin. Neurobiol.* **27**, 118–126.
- Cho, Y., Sloutsky, R., Naegle, K.M., and Cavalli, V. (2013). Injury-induced HDAC5 nuclear export is essential for axon regeneration. *Cell* **155**, 894–908.
- Cho, Y., Park, D., and Cavalli, V. (2015). Filamin A is required in injured axons for HDAC5 activity and axon regeneration. *J. Biol. Chem.* **290**, 22759–22770.
- Costigan, M., Befort, K., Karchewski, L., Griffin, R.S., D'Urso, D., Allchorne, A., Sitariski, J., Mannion, J.W., Pratt, R.E., and Woolf, C.J. (2002). Replicate high-density rat genome oligonucleotide microarrays reveal hundreds of regulated genes in the dorsal root ganglion after peripheral nerve injury. *BMC Neurosci.* **3**, 16.
- Cui, Q., Shi, H., Ye, P., Li, L., Qu, Q., Sun, G., Sun, G., Lu, Z., Huang, Y., Yang, C.G., et al. (2017). m6A RNA methylation regulates the self-renewal and tumorigenesis of glioblastoma stem cells. *Cell Rep.* **18**, 2622–2634.
- Desrosiers, R.C., Friderici, K.H., and Rottman, F.M. (1975). Characterization of Novikoff hepatoma mRNA methylation and heterogeneity in the methylated 5' terminus. *Biochemistry* **14**, 4367–4374.
- Di Maio, A., Skuba, A., Himes, B.T., Bhagat, S.L., Hyun, J.K., Tessler, A., Bishop, D., and Son, Y.J. (2011). In vivo imaging of dorsal root regeneration: rapid immobilization and presynaptic differentiation at the CNS/PNS border. *J. Neurosci.* **31**, 4569–4582.
- Dobin, A., Davis, C.A., Schlesinger, F., Drenkow, J., Zaleski, C., Jha, S., Batut, P., Chaisson, M., and Gingeras, T.R. (2013). STAR: ultrafast universal RNA-seq aligner. *Bioinformatics* **29**, 15–21.
- Dominissini, D., Moshitch-Moshkovitz, S., Schwartz, S., Salmon-Divon, M., Ungar, L., Osenberg, S., Cesarkas, K., Jacob-Hirsch, J., Amariglio, N., Kupiec, M., et al. (2012). Topology of the human and mouse m6A RNA methylomes revealed by m6A-seq. *Nature* **485**, 201–206.
- Donnelly, C.J., Park, M., Spillane, M., Yoo, S., Pacheco, A., Gomes, C., Vuppalachchi, D., McDonald, M., Kim, H.H., Merianda, T.T., et al. (2013). Axonally synthesized  $\beta$ -actin and GAP-43 proteins support distinct modes of axonal growth. *J. Neurosci.* **33**, 3311–3322.
- Duan, X., Qiao, M., Bei, F., Kim, I.J., He, Z., and Sanes, J.R. (2015). Subtype-specific regeneration of retinal ganglion cells following axotomy: effects of osteopontin and mTOR signaling. *Neuron* **85**, 1244–1256.
- Fagoe, N.D., Attwell, C.L., Kouwenhoven, D., Verhaagen, J., and Mason, M.R. (2015). Overexpression of ATF3 or the combination of ATF3, c-Jun, STAT3 and Smad1 promotes regeneration of the central axon branch of sensory neurons but without synergistic effects. *Hum. Mol. Genet.* **24**, 6788–6800.
- Finelli, M.J., Wong, J.K., and Zou, H. (2013). Epigenetic regulation of sensory axon regeneration after spinal cord injury. *J. Neurosci.* **33**, 19664–19676.
- Gaub, P., Joshi, Y., Wuttke, A., Naumann, U., Schnichels, S., Heiduschka, P., and Di Giovanni, S. (2011). The histone acetyltransferase p300 promotes intrinsic axonal regeneration. *Brain* **134**, 2134–2148.
- Geula, S., Moshitch-Moshkovitz, S., Dominissini, D., Mansour, A.A., Kol, N., Salmon-Divon, M., Hershkovitz, V., Peer, E., Mor, N., Manor, Y.S., et al. (2015). Stem cells. m6A mRNA methylation facilitates resolution of naïve pluripotency toward differentiation. *Science* **347**, 1002–1006.
- Gilbert, W.V., Bell, T.A., and Schaening, C. (2016). Messenger RNA modifications: Form, distribution, and function. *Science* **352**, 1408–1412.
- Goodman, C.A., Mabrey, D.M., Frey, J.W., Miu, M.H., Schmidt, E.K., Pierre, P., and Hornberger, T.A. (2011). Novel insights into the regulation of skeletal muscle protein synthesis as revealed by a new nonradioactive in vivo technique. *FASEB J.* **25**, 1028–1039.
- Guo, J.U., Su, Y., Zhong, C., Ming, G.L., and Song, H. (2011). Emerging roles of TET proteins and 5-hydroxymethylcytosines in active DNA demethylation and beyond. *Cell Cycle* **10**, 2662–2668.
- Haussmann, I.U., Bodi, Z., Sanchez-Moran, E., Mongan, N.P., Archer, N., Fray, R.G., and Soller, M. (2016). m6A potentiates Sxl alternative pre-mRNA splicing for robust Drosophila sex determination. *Nature* **540**, 301–304.
- Jankowski, M.P., McIlwrath, S.L., Jing, X., Cornuet, P.K., Salerno, K.M., Koerber, H.R., and Albers, K.M. (2009). Sox11 transcription factor modulates peripheral nerve regeneration in adult mice. *Brain Res.* **1256**, 43–54.
- Jia, G., Fu, Y., Zhao, X., Dai, Q., Zheng, G., Yang, Y., Yi, C., Lindahl, T., Pan, T., Yang, Y.G., and He, C. (2011). N6-methyladenosine in nuclear RNA is a major substrate of the obesity-associated FTO. *Nat. Chem. Biol.* **7**, 885–887.
- Jung, H., Yoon, B.C., and Holt, C.E. (2012). Axonal mRNA localization and local protein synthesis in nervous system assembly, maintenance and repair. *Nat. Rev. Neurosci.* **13**, 308–324.
- Ke, S., Alemu, E.A., Mertens, C., Gantman, E.C., Fak, J.J., Mele, A., Haripal, B., Zucker-Scharff, I., Moore, M.J., Park, C.Y., et al. (2015). A majority of m6A residues are in the last exons, allowing the potential for 3' UTR regulation. *Genes Dev.* **29**, 2037–2053.
- Kim, Y.S., Anderson, M., Park, K., Zheng, Q., Agarwal, A., Gong, C., Saijilafu, Young, L., He, S., LaVinka, P.C., et al. (2016). Coupled activation of primary sensory neurons contributes to chronic pain. *Neuron* **91**, 1085–1096.
- Lence, T., Akhtar, J., Bayer, M., Schmid, K., Spindler, L., Ho, C.H., Kreim, N., Andrade-Navarro, M.A., Poeck, B., Helm, M., and Roignant, J.Y. (2016). m6A modulates neuronal functions and sex determination in Drosophila. *Nature* **540**, 242–247.
- Li, H., Handsaker, B., Wysoker, A., Fennell, T., Ruan, J., Homer, N., Marth, G., Abecasis, G., and Durbin, R.; 1000 Genome Project Data Processing Subgroup (2009). The Sequence Alignment/Map format and SAMtools. *Bioinformatics* **25**, 2078–2079.
- Li, X., Xiong, X., and Yi, C. (2016). Epitranscriptome sequencing technologies: decoding RNA modifications. *Nat. Methods* **14**, 23–31.

- Li, A., Chen, Y.S., Ping, X.L., Yang, X., Xiao, W., Yang, Y., Sun, H.Y., Zhu, Q., Baidya, P., Wang, X., et al. (2017a). Cytoplasmic m6A reader YTHDF3 promotes mRNA translation. *Cell Res.* *27*, 444–447.
- Li, H.B., Tong, J., Zhu, S., Batista, P.J., Duffy, E.E., Zhao, J., Bailis, W., Cao, G., Kroehling, L., Chen, Y., et al. (2017b). m6A mRNA methylation controls T cell homeostasis by targeting the IL-7/STAT5/SOCS pathways. *Nature* *548*, 338–342.
- Li, L., Zang, L., Zhang, F., Chen, J., Shen, H., Shu, L., Liang, F., Feng, C., Chen, D., Tao, H., et al. (2017c). Fat mass and obesity-associated (FTO) protein regulates adult neurogenesis. *Hum. Mol. Genet.* *26*, 2398–2411.
- Lin, S., Choe, J., Du, P., Triboulet, R., and Gregory, R.I. (2016). The m(6)A methyltransferase METTL3 promotes translation in human cancer cells. *Mol. Cell* *62*, 335–345.
- Linder, B., Grozhik, A.V., Olarerin-George, A.O., Meydan, C., Mason, C.E., and Jaffrey, S.R. (2015). Single-nucleotide-resolution mapping of m6A and m6Am throughout the transcriptome. *Nat. Methods* *12*, 767–772.
- Liu, K., Lu, Y., Lee, J.K., Samara, R., Willenberg, R., Sears-Kraxberger, I., Tedeschi, A., Park, K.K., Jin, D., Cai, B., et al. (2010). PTEN deletion enhances the regenerative ability of adult corticospinal neurons. *Nat. Neurosci.* *13*, 1075–1081.
- Liu, K., Tedeschi, A., Park, K.K., and He, Z. (2011). Neuronal intrinsic mechanisms of axon regeneration. *Annu. Rev. Neurosci.* *34*, 131–152.
- Meijering, E., Jacob, M., Sarria, J.C., Steiner, P., Hirling, H., and Unser, M. (2004). Design and validation of a tool for neurite tracing and analysis in fluorescence microscopy images. *Cytometry A* *58*, 167–176.
- Meyer, K.D., Saletore, Y., Zumbo, P., Elemento, O., Mason, C.E., and Jaffrey, S.R. (2012). Comprehensive analysis of mRNA methylation reveals enrichment in 3' UTRs and near stop codons. *Cell* *149*, 1635–1646.
- Meyer, K.D., Patil, D.P., Zhou, J., Zinoviev, A., Skabkin, M.A., Elemento, O., Pestova, T.V., Qian, S.B., and Jaffrey, S.R. (2015). 5' UTR m(6)A promotes cap-independent translation. *Cell* *163*, 999–1010.
- Molinie, B., Wang, J., Lim, K.S., Hillebrand, R., Lu, Z.X., Van Wittenberghe, N., Howard, B.D., Daneshvar, K., Mullen, A.C., Dedon, P., et al. (2016). m(6)A-LAIC-seq reveals the census and complexity of the m(6)A epitranscriptome. *Nat. Methods* *13*, 692–698.
- Moore, D.L., and Goldberg, J.L. (2011). Multiple transcription factor families regulate axon growth and regeneration. *Dev. Neurobiol.* *71*, 1186–1211.
- Moore, M.J., Zhang, C., Gantman, E.C., Mele, A., Darnell, J.C., and Darnell, R.B. (2014). Mapping Argonaute and conventional RNA-binding protein interactions with RNA at single-nucleotide resolution using HITS-CLIP and CIMS analysis. *Nat. Protoc.* *9*, 263–293.
- Park, K.K., Liu, K., Hu, Y., Smith, P.D., Wang, C., Cai, B., Xu, B., Connolly, L., Kramvis, I., Sahin, M., and He, Z. (2008). Promoting axon regeneration in the adult CNS by modulation of the PTEN/mTOR pathway. *Science* *322*, 963–966.
- Perlson, E., Hanz, S., Ben-Yaakov, K., Segal-Ruder, Y., Seger, R., and Fainzilber, M. (2005). Vimentin-dependent spatial translocation of an activated MAP kinase in injured nerve. *Neuron* *45*, 715–726.
- Picelli, S., Faridani, O.R., Björklund, A.K., Winberg, G., Sagasser, S., and Sandberg, R. (2014). Full-length RNA-seq from single cells using Smart-seq2. *Nat. Protoc.* *9*, 171–181.
- Puttagunta, R., Tedeschi, A., Sória, M.G., Hervera, A., Lindner, R., Rathore, K.I., Gaub, P., Joshi, Y., Nguyen, T., Schmandke, A., et al. (2014). PCAF-dependent epigenetic changes promote axonal regeneration in the central nervous system. *Nat. Commun.* *5*, 3527.
- Quinlan, A.R., and Hall, I.M. (2010). BEDTools: a flexible suite of utilities for comparing genomic features. *Bioinformatics* *26*, 841–842.
- Rishal, I., and Fainzilber, M. (2014). Axon-soma communication in neuronal injury. *Nat. Rev. Neurosci.* *15*, 32–42.
- Schmidt, E.K., Clavarino, G., Ceppi, M., and Pierre, P. (2009). SUNSET, a nonradioactive method to monitor protein synthesis. *Nat. Methods* *6*, 275–277.
- Seiffers, R., Mills, C.D., and Woolf, C.J. (2007). ATF3 increases the intrinsic growth state of DRG neurons to enhance peripheral nerve regeneration. *J. Neurosci.* *27*, 7911–7920.
- Shi, H., Wang, X., Lu, Z., Zhao, B.S., Ma, H., Hsu, P.J., Liu, C., and He, C. (2017). YTHDF3 facilitates translation and decay of N6-methyladenosine-modified RNA. *Cell Res.* *27*, 315–328.
- Shin, J.E., Cho, Y., Beirowski, B., Milbrandt, J., Cavalli, V., and DiAntonio, A. (2012). Dual leucine zipper kinase is required for retrograde injury signaling and axonal regeneration. *Neuron* *74*, 1015–1022.
- Shin, J.E., Geisler, S., and DiAntonio, A. (2014). Dynamic regulation of SCG10 in regenerating axons after injury. *Exp. Neurol.* *252*, 1–11.
- Smith, D.S., and Skene, J.H. (1997). A transcription-dependent switch controls competence of adult neurons for distinct modes of axon growth. *J. Neurosci.* *17*, 646–658.
- Song, H., and Poo, M. (2001). The cell biology of neuronal navigation. *Nat. Cell Biol.* *3*, E81–E88.
- Su, Y., Shin, J., Zhong, C., Wang, S., Roychowdhury, P., Lim, J., Kim, D., Ming, G.L., and Song, H. (2017). Neuronal activity modifies the chromatin accessibility landscape in the adult brain. *Nat. Neurosci.* *20*, 476–483.
- Tedeschi, A., and Bradke, F. (2017). Spatial and temporal arrangement of neuronal intrinsic and extrinsic mechanisms controlling axon regeneration. *Curr. Opin. Neurobiol.* *42*, 118–127.
- Trakhtenberg, E.F., and Goldberg, J.L. (2012). Epigenetic regulation of axon and dendrite growth. *Front. Mol. Neurosci.* *5*, 24.
- van Niekerk, E.A., Tuszyński, M.H., Lu, P., and Dulin, J.N. (2016). Molecular and cellular mechanisms of axonal regeneration after spinal cord injury. *Mol. Cell. Proteomics* *15*, 394–408.
- Walters, B.J., Meraldo, V., Gillon, C.J., Yip, M., Neve, R.L., Boyce, F.M., Frankland, P.W., and Josselyn, S.A. (2017). The role of the RNA demethylase FTO (fat mass and obesity-associated) and mRNA methylation in hippocampal memory formation. *Neuropsychopharmacology* *42*, 1502–1510.
- Wang, Y., Li, Y., Toth, J.I., Petroski, M.D., Zhang, Z., and Zhao, J.C. (2014). N6-methyladenosine modification destabilizes developmental regulators in embryonic stem cells. *Nat. Cell Biol.* *16*, 191–198.
- Wang, X., Zhao, B.S., Roundtree, I.A., Lu, Z., Han, D., Ma, H., Weng, X., Chen, K., Shi, H., and He, C. (2015). N(6)-methyladenosine modulates messenger RNA translation efficiency. *Cell* *161*, 1388–1399.
- Wang, X., Huang, J., Zou, T., and Yin, P. (2017). Human m6A writers: Two subunits, 2 roles. *RNA Biol.* *14*, 300–304.
- Weng, Y.L., An, R., Shin, J., Song, H., and Ming, G.L. (2013). DNA modifications and neurological disorders. *Neurotherapeutics* *10*, 556–567.
- Weng, Y.L., Joseph, J., An, R., Song, H., and Ming, G.L. (2016). Epigenetic regulation of axonal regenerative capacity. *Epigenomics* *8*, 1429–1442.
- Weng, Y.L., An, R., Cassin, J., Joseph, J., Mi, R., Wang, C., Zhong, C., Jin, S.G., Pfeifer, G.P., Bellacosa, A., et al. (2017). An intrinsic epigenetic barrier for functional axon regeneration. *Neuron* *94*, 337–346.e6.
- Widagdo, J., Zhao, Q.Y., Kempen, M.J., Tan, M.C., Ratnu, V.S., Wei, W., Leighton, L., Spadaro, P.A., Edson, J., Anggono, V., and Bredy, T.W. (2016). Experience-dependent accumulation of N6-methyladenosine in the prefrontal cortex is associated with memory processes in mice. *J. Neurosci.* *36*, 6771–6777.
- Wong, J.K., and Zou, H. (2014). Reshaping the chromatin landscape after spinal cord injury. *Front. Biol. (Beijing)* *9*, 356–366.
- Wright, M.C., Mi, R., Connor, E., Reed, N., Vyas, A., Alspalter, M., Coppola, G., Geschwind, D.H., Brushart, T.M., and Höke, A. (2014). Novel roles for osteopontin and clusterin in peripheral motor and sensory axon regeneration. *J. Neurosci.* *34*, 1689–1700.
- Yao, B., Christian, K.M., He, C., Jin, P., Ming, G.L., and Song, H. (2016). Epigenetic mechanisms in neurogenesis. *Nat. Rev. Neurosci.* *17*, 537–549.
- Yoon, K.J., Ringeling, F.R., Vissers, C., Jacob, F., Pokrass, M., Jimenez-Cyrus, D., Su, Y., Kim, N.S., Zhu, Y., Zheng, L., et al. (2017). Temporal control of mammalian cortical neurogenesis by m6A methylation. *Cell* *171*, 877–889.e17.

- Yu, J., Chen, M., Huang, H., Zhu, J., Song, H., Zhu, J., Park, J., and Ji, S.J. (2017). Dynamic m6A modification regulates local translation of mRNA in axons. *Nucleic Acids Res.* <https://doi.org/10.1093/nar/gkx1182>.
- Zhang, C., and Darnell, R.B. (2011). Mapping in vivo protein-RNA interactions at single-nucleotide resolution from HITS-CLIP data. *Nat. Biotechnol.* *29*, 607–614.
- Zhang, C., Chen, Y., Sun, B., Wang, L., Yang, Y., Ma, D., Lv, J., Heng, J., Ding, Y., Xue, Y., et al. (2017). m6A modulates haematopoietic stem and progenitor cell specification. *Nature* *549*, 273–276.
- Zhao, B.S., Roundtree, I.A., and He, C. (2017a). Post-transcriptional gene regulation by mRNA modifications. *Nat. Rev. Mol. Cell Biol.* *18*, 31–42.
- Zhao, B.S., Wang, X., Beadell, A.V., Lu, Z., Shi, H., Kuuspalu, A., Ho, R.K., and He, C. (2017b). m6A-dependent maternal mRNA clearance facilitates zebrafish maternal-to-zygotic transition. *Nature* *542*, 475–478.
- Zheng, G., Dahl, J.A., Niu, Y., Fedorcsak, P., Huang, C.M., Li, C.J., Vågbo, C.B., Shi, Y., Wang, W.L., Song, S.H., et al. (2013). ALKBH5 is a mammalian RNA demethylase that impacts RNA metabolism and mouse fertility. *Mol. Cell* *49*, 18–29.
- Zhou, J., Wan, J., Gao, X., Zhang, X., Jaffrey, S.R., and Qian, S.B. (2015). Dynamic m(6)A mRNA methylation directs translational control of heat shock response. *Nature* *526*, 591–594.

## STAR★METHODS

## KEY RESOURCES TABLE

REAGENT or RESOURCE	SOURCE	IDENTIFIER
<b>Antibodies</b>		
Mouse anti-Puromycin	Millipore	MABE343; RRID: AB_2566826
Rabbit anti-ATF3	Santa Cruz	sc-188; RRID: AB_2258513
Rabbit anti-PGP9.5	AbD Serotec	7863-0504; RRID: AB_2210505
Rabbit anti-SCG10	Novus Biologicals	NBP1-49461; RRID: AB_10011569
Rabbit anti-m6A	Synaptic systems	202003; RRID: AB_2279214
Rabbit anti-Mettl14	Proteintech	26158-1-AP; N/A
Rabbit anti-cleaved caspase 3	Invitrogen	9H19L2; RRID: AB_2532293
Rabbit anti-GAPDH	Abcam	Ab9485; RRID: AB_307275
Mouse anti-GAPDH	EMD Millipore	AB2302; RRID: AB_10615768
Rabbit anti-YTHDF1	Proteintech	17479-1-AP; RRID: AB_2217473
Rabbit anti-pS6	Cell Signaling	4858; RRID: AB_916156
Mouse anti-SMI32	BioLegend	801701; RRID: AB_2564642
Mouse anti-Tuj1	BioLegend	801202; RRID: AB_10063408
Mouse anti-Glutamine Synthetase	Santa Cruz	sc-74430; RRID: AB_1127501
Cy2-, Cy3- or Cy5-conjugated secondary antibodies	Jackson ImmunoResearch	705-225-147, RRID: AB_2307341; 711-165-152, RRID: AB_2307443; 715-175-150, RRID: AB_2340819
HRP-conjugated goat anti-mouse IgG	Santa Cruz	sc-2031; RRID: AB_631737
HRP-conjugated goat anti-rabbit IgG	Santa Cruz	sc-2004; RRID: AB_631746
<b>Chemicals, Peptides, and Recombinant Proteins</b>		
TRIzol	Thermo Fisher	15596018
Formaldehyde	Sigma-Aldrich	F8775-25ML
N <sup>6</sup> -Methyladenosine	Sigma-Aldrich	M2780
Puromycin Dihydrochloride	Sigma-Aldrich	P8833-25MG
Cholera Toxin B Subunit, FITC Conjugate	Sigma-Aldrich	C1655-5MG
Fluoro-Max fluorescent beads	Invitrogen	B0100
<b>Critical Commercial Assays</b>		
Collagenase	Invitrogen	17100017
Zamboni's fixative	Newcomer Supply	1459
RNA fragmentation reagents	Thermo Fisher	AM8740
RNA clean and concentrator	Zymo Research	R1017
SMARTScribe reverse transcriptase	Clontech	639537
SuperSignal West Dura Extended Duration Substrate	Thermo Fisher	34075
Protein A Dynabeads	Thermo Fisher	10002D
Fast SYBR Green Master Mix	ABI	4385612
FastAP	Thermo Fisher	EF0651
<i>E. coli</i> Poly(A) Polymerase	NEB	M0276S
Proteinase K	Thermo Fisher	25530049
SUPERase In RNase Inhibitor	Thermo Fisher	AM2696
mMessage mMachine T7 Ultra kit	Thermo Fisher	AM1345
Dynabeads Oligo (dT) <sub>25</sub>	Thermo Fisher	61006
SMARTScribe reverse transcriptase	Clontech	639537
Advantage 2 Polymerase Mix	Clontech	639201

(Continued on next page)

**Continued**

REAGENT or RESOURCE	SOURCE	IDENTIFIER
KAPA HiFi PCR Kits	Kapa Biosystems	KK2502
Agencourt AMPure XP	Beckman Coulter	A63880
EZ-Tn5 Transposase	Epicenter	TNP92110
Rabbit IgG	Cell Signaling	2729
Deposited Data		
Raw and analyzed data	This paper	GEO: GSE106423
Experimental Models: Organisms/Strains		
Mouse: Adult C57Bl6/J	Charles River	N/A
Mouse: <i>Mettl14<sup>fl/fl</sup></i> C57Bl6/J	<a href="#">Yoon et al., 2017</a>	N/A
Mouse: <i>Ythdf1<sup>-/-</sup></i> C57Bl6/J	C.H., unpublished data	N/A
Mouse: <i>Pten<sup>fl/fl</sup></i> mice C57Bl6/J	<a href="#">Park et al., 2008</a>	N/A
Mouse: <i>Pirt-GCaMP3</i> C57Bl6/J	<a href="#">Weng et al., 2017</a>	N/A
Mouse: <i>Synapsin1-Cre</i>	Charles River	N/A
Oligonucleotides		
qPCR primers	This paper	See <a href="#">Table S5</a>
Control shRNA: CCTAAGGTTAAGTCGCCCTC	<a href="#">Wang et al., 2014</a>	N/A
Mettl14 shRNA: GCATTGGTGCTGTGTTAAATA	<a href="#">Wang et al., 2014</a>	N/A
Recombinant DNA		
AAV2/9 virus	<a href="#">Guo et al., 2011</a>	N/A
AAV2 virus	<a href="#">Weng et al., 2017</a>	N/A
AAV2/9 GFP-Cre virus	UPenn Vector Core	V1656
Software and Algorithms		
NeuronJ	<a href="#">Meijering et al., 2004</a>	RRID: SCR_002074; <a href="https://imagescience.org/meijering/software/neuronj/">https://imagescience.org/meijering/software/neuronj/</a>
ImageJ	NIH	RRID: SCR_003070; <a href="https://imagej.nih.gov/ij/">https://imagej.nih.gov/ij/</a>
STAR	<a href="#">Dobin et al., 2013</a>	RRID: SCR_005622; <a href="https://github.com/alexdobin/STAR">https://github.com/alexdobin/STAR</a>
CIMS	<a href="#">Zhang and Darnell, 2011</a>	<a href="https://github.com/chaolinzhanglab/ctk/tree/v1.0.3">https://github.com/chaolinzhanglab/ctk/tree/v1.0.3</a>
Trimmomatic	<a href="#">Bolger et al., 2014</a>	RRID: SCR_011848; <a href="http://www.usadellab.org/cms/?page=trimmomatic">http://www.usadellab.org/cms/?page=trimmomatic</a>
Samtools	<a href="#">Li et al., 2009</a>	RRID: SCR_002105; <a href="http://samtools.sourceforge.net/">http://samtools.sourceforge.net/</a>
Bedtools	<a href="#">Quinlan and Hall, 2010</a>	RRID: SCR_006646; <a href="http://bedtools.readthedocs.io/en/latest/">http://bedtools.readthedocs.io/en/latest/</a>
Other		
30 gauge syringe	Hamilton	N/A
Ultra-fine hemostatic forceps	F.S.T.	13021-12
Radiant heat light source (model 33 Analgesia Meter)	IITC/Life Science Instruments	N/A
Confocal Microscope	Zeiss	N/A
Applied Biosystems 7500	Thermo Fisher	N/A
Dumont number 5 forceps	Roboz	N/A
Hybond-N+ membrane	GE Healthcare	RPN2020N
UV stratalinker 1800	Stratagene	N/A
10% Mini-PROTEAN TGX Precast Protein Gels	Bio-rad	4561033
Trans-Blot Turbo Mini PVDF Transfer Packs	Bio-rad	1704156
Trans-Blot Turbo Transfer Starter System	Bio-rad	1704155
Dounce tissue grinder set	Sigma	D9938-1SET
Bioruptor plus	Diagenode	N/A

## CONTACT FOR REAGENT AND RESOURCE SHARING

Further information and requests for resources and reagents should be directed to and will be fulfilled by the Lead Contact, Guo-li Ming ([gming@penncmedicine.upenn.edu](mailto:gming@penncmedicine.upenn.edu)). There are no restrictions on any data or materials presented in this paper.

## EXPERIMENTAL MODEL AND SUBJECT DETAILS

### Animals

All animal procedures used in this study were performed in accordance with the protocol approved by the Institutional Animal Care and Use Committee of Johns Hopkins University School of Medicine, University of Pennsylvania School of Medicine, and The Hong Kong University of Science and Technology. Six mouse lines were used for this study: C57Bl6/J mice, *Pirt-GCaMP3* mice (Kim et al., 2016), *Mettl14<sup>fl/fl</sup>* mice (Yoon et al., 2017); *Syn1-Cre* mice (JAX 003966), *Ythdf1<sup>-/-</sup>* mice (manuscript in preparation), and *Pten<sup>fl/fl</sup>* mice (Bonaguidi et al., 2011). Adult mice (6-8 weeks) were used. Housing and husbandry conditions followed standard settings. Experimental and control mice were male littermates housed together before the experiment.

## METHOD DETAILS

### AAV constructs

The recombinant AAV2/9 vectors for Cre and GFP were from the UPenn Vector Core. AAV2 for shRNA-control and shRNA-Mettl14 were constructed and prepared in house.

### Animal surgery

Intrathecal injection of AAV2/9 was performed in adult 6-8 weeks old male mice as previously described (Weng et al., 2017). Briefly, 3  $\mu$ L of viral solution was injected into the cerebrospinal fluid between vertebrae L5 and L6 using a 30 gauge Hamilton syringe slowly over 2 min followed an additional 2-minute wait to allow the fluid to diffuse. Following the injection, the mice were left undisturbed for 3 weeks for recovery and for complete dissemination of the virus.

For sciatic nerve lesion (SNL), mice were anesthetized and a small incision was made on the skin at the mid-thigh level. The sciatic nerve was exposed after opening the fascial plane between the gluteus superficialis and biceps femoris muscles. The nerve was carefully freed from surrounding connective tissue and then crushed for 15 s at 3 clicks of ultra-fine hemostatic forceps (F.S.T. 13021-12). The crush site was labeled by Fluoro-Max dyed blue aqueous fluorescent particles (Thermo Fisher; B0100; Figure S4D). Skin was then closed with two suture clips. For the sham surgery (the naive conditions), the sciatic nerve in the contralateral side was exposed and mobilized but left uninjured. For the thermal withdrawal test and skin biopsy experiments, the saphenous nerve was ligated and transected above the knee region after sciatic nerve crush, so that the hindpaw epidermis could only be innervated by regenerating sciatic nerve axons.

For optic nerve injury, the procedure was performed as previously described (Park et al., 2008). Briefly, individual AAV-shRNA-control or AAV-shRNA-Mettl14 was mixed with AAV-Cre and intravitreally injected to the left eye of adult WT or *Pten<sup>fl/fl</sup>* mice. Two weeks after viral injection, the left optic nerve was exposed intraorbitally and crushed with jeweler's forceps (Dumont number 5; Roboz) for 5 s, approximately 1 mm behind the optic disc. To visualize regenerating axons, RGC axons in the optic nerve were anterogradely labeled by 1  $\mu$ l of cholera toxin  $\beta$  subunit (CTB; 2  $\mu$ g/ $\mu$ l; Invitrogen) 12 days after injury. Animals were fixed by 4% PFA 2 days after CTB injection in the eye. Quantification of regenerating axons was also performed according the previously described method (Park et al., 2008).

### DRG cultures and neurite outgrowth assay

DRG primary culture was performed as previously described (Chen et al., 2017). Briefly, mice were anesthetized and perfused with sterile PBS. L4-L6 DRGs were dissected, washed in cold HBSS medium and then digested in 0.1% collagenase (Invitrogen; 17100017) in HBSS for 90 min. After triturated into single cell suspension, DRG neurons were precipitated at room temperature for 20 min and plated on a coated culture dish. Cultures were infected with AAV co-expressing Cre and different shRNAs (Key Resources Table). For re-plating, DRG neurons cultured with AAV for 10 days were gently flushed, resuspended and replated on a coated culture dish. The replated neurons were cultured for another one day and fixed for Tuj1 staining. The average lengths of longest neurites from each DRG neurons were measured and quantified by ImageJ.

### m<sup>6</sup>A-SMART-seq

mRNA from total RNA of adult mouse DRGs was purified with Dynabeads Oligo (dT)<sub>25</sub> (Thermo Fisher; 61006). Five  $\mu$ g of anti-m<sup>6</sup>A polyclonal antibody (Synaptic Systems; 202003) was conjugated to Dynabeads Protein A (Thermo Fisher; 10001D) overnight at 4°C. A total of 150 ng of mRNA was then incubated with the antibody/beads in 1x IP buffer (10 mM Tris-HCl, 150 mM NaCl, and 0.1% (vol/vol) Igepal CA-630), supplemented with 200 U SUPERase In RNase Inhibitor (Thermo Fisher; AM2696), for 2 hr at 4°C. After incubation, the beads were washed 3 times with IP buffer and the m<sup>6</sup>A RNA was eluted twice with 6.7 mM N<sup>6</sup>-Methyladenosine (Sigma-Aldrich; M2780) in 1x IP buffer. The eluted RNA was extracted with Trizol reagent (Thermo Fisher; 15596018) and recovered

by RNA Clean and Concentrator-5 spin columns (Zymo; R1015). The equivalent amount of input and m<sup>6</sup>A-IPed RNA were prepared for library generation using the SMART-seq protocol as described (Picelli et al., 2014). Two biological replicates of naive and SNL conditions were sequenced using Illumina NextSeq 500.

### m<sup>6</sup>A-CLIP-SMART-seq

A total of 150 ng mRNA was first fragmented to ~100 nt by RNA Fragmentation Reagent (Thermo Fisher; AM8740) at 70°C for 8 min. After the reaction was stopped by 100 mM EDTA, the RNA mixtures were then directly diluted to 450 μL CLIP buffer (150 mM NaCl, 0.1% NP-40, 10 mM Tris-HCl (pH 7.4)) with 5 μg anti-m<sup>6</sup>A polyclonal antibody (Synaptic Systems; 202003) and incubated at 4°C for 2 hrs. Anti-m<sup>6</sup>A antibody - RNA interactions were stabilized with UV crosslinking (254 nm, 150 mJ/cm<sup>2</sup>) twice in a Stratalinker (Agilent). Antibody-RNA complexes were then precipitated with 50 μL Protein A/G beads (Thermo Scientific) for 2 hr at 4°C, followed by two stringent washes (50 mM Tris, pH 7.4, 1 M NaCl, 1 mM EDTA, 1% NP-40, 0.1% SDS) and two CLIP buffer washes. After dephosphorylation with 10 U FastAP (Thermo Fisher; EF0652) at 10 min at room temperature and polyadenylation with 5U *E. coli* Poly(A) Polymerase (NEB, M0276S) for 15 min at room temperature on beads, the RNA was then eluted by treatment with proteinase K (Thermo Scientific; 25530049) at 37°C for 1 hr. The eluted RNA was extracted with Trizol reagent (Thermo Fisher; 15596018) and recovered by RNA Clean and Concentrator-5 spin columns (Zymo; R1015). The m<sup>6</sup>A CLIP library was prepared using a modified SMART-seq2 protocol without tagmentation. Briefly, RNA was first primed with customized dT primer (GTCTCGTGGGCTCGGA GATGTGTATAAGAGACAG T<sub>30</sub>VN) and incubated with RT master mix containing customized TSO primer (TCGTCGGCAGCGTCA GATGTGTATAAGAGACArGrGrG) at 42°C for 1.5 hr. Libraries were PCR amplified for 19 cycles, size selected via BluePippin and sequenced on Illumina NextSeq 500.

### RNA-seq

Total RNA of L4/L5 DRGs was isolated from WT and Syn1-Cre;*Mettl14*<sup>fl/fl</sup> cKO mice, extracted with Trizol reagent (Thermo Fisher; 15596018) and recovered by RNA Clean and Concentrator-5 spin columns (Zymo; R1015). The RNA-seq library was prepared using the Smart-seq2 protocol. The distribution of fragment sizes was verified. Libraries of three biological replicates under different conditions were uniquely barcoded, pooled at equimolar concentrations, and sequenced on Illumina NextSeq 500 (Su et al., 2017).

### Analysis m<sup>6</sup>A-SMART-Seq and RNA-seq

Adapters were trimmed from original reads using Trimmomatic and low-quality reads were removed. The remaining reads were then mapped to the mouse genome (mm10) using STAR aligner (Dobin et al., 2013). To measure the relative m<sup>6</sup>A level per gene, the ratio of m<sup>6</sup>A IP/ Input was first calculated. The Z scores were then obtained by comparing the ratios (m<sup>6</sup>A IP/ Input) to the mean of the group to reflect the relative m<sup>6</sup>A level per gene on a transcriptome-wide scale (Batista et al., 2014). GAPDH is barely methylated (validated by m<sup>6</sup>A-MeRIP Q-PCR) with Z score < 0. We set Z score > 0 as a threshold to obtain genes with modest to high m<sup>6</sup>A levels. Shared m<sup>6</sup>A-tagged genes in two biological replicates were identified as high confidence m<sup>6</sup>A-tagged transcripts for downstream analysis. The gene list of RAGs was obtained from the magenta module in the previous study (Chandran et al., 2016). For the comparison of m<sup>6</sup>A transcriptomes between naive and SNL D1 conditions, m<sup>6</sup>A-tagged transcript levels were presented as mean TPM (Mean transcripts per kilobase million). The top 400 differentially m<sup>6</sup>A-tagged genes were uploaded to the Panther Classification System for a statistical overrepresentation test.

### Analysis of m<sup>6</sup>A-CLIP-SMART-seq

Adapters, and the first three nucleotides of the sequencing read (derived from the TSO oligo) were removed by Trimmomatic. The remaining reads (> 20 nt) were then mapped to the mouse genome (mm10) using STAR aligner (-outFilterMultimapNmax 1- outFilterMismatchNoverLmax 0.08-alignEndsType EndToEnd). After removal of PCR duplicates, uniquely mapped reads were used for CIMS analysis similar to previous studies (Linder et al., 2015; Moore et al., 2014; Zhang and Darnell, 2011). All mutations were considered as signals. The number of overlapping unique tags (*k*) and the number of tags with mutations (*m*) at the position were determined using the CIMS algorithm. The *m/k* was restricted to between 1% and 50% to reduce noise and remove SNP and mis-mapping artifacts. Only m<sup>6</sup>A residues in DRACH consensus sequence were considered for the downstream analysis. The list of genes with differential m<sup>6</sup>A-tag numbers (gain > 3 or lost > 2) was uploaded to the Panther Classification System for a statistical overrepresentation test.

### m<sup>6</sup>A-MeRIP Q-PCR

The m<sup>6</sup>A-modified control spike-in RNA (eGFP, 0.7 kb) was synthesized by *in vitro* transcription using the mMessage mMachine T7 Ultra kit (Thermo Fisher; AM1345). A total of 150 ng of input mRNA was mixed with 10 pg of control spike-in RNA and subjected to m<sup>6</sup>A-IP as described above. Immunoprecipitated RNA was purified and reverse-transcribed with Oligo (dT) primer using SMARTScribe Reverse Transcriptase (Clontech; 639537). Indicated genes were analyzed by Q-PCR using Fast SYBR Green Master Mix (Thermo Fisher; 4385612) and normalized to the spike-in eGFP RNA levels. Relative fold change was calculated as the ratio of normalized transcript levels between naive and SNL D1 conditions. Primer sequences are listed in Table S3.

### m<sup>6</sup>A dot blot analysis

mRNA was harvested from homogenized WT and *Mettl14* cKO DRGs using Dynabeads mRNA Direct Purification Kit (Ambion; 61011). Three biological replicates were pooled for each sample to ensure sufficient concentration of mRNA. Duplicates of 100 ng mRNA per 1  $\mu$ L were applied to an Amersham Hybond-N<sup>+</sup> membrane (GE Healthcare) as previously described (Yoon et al., 2017). UV crosslinking of RNA to the membrane was performed by running the auto-crosslink program twice in Stratalinker 2400. The membrane was then washed in PBST three times and blocked with 5% skim milk in PBST for 2 hr. After an additional PBST wash, primary anti-m<sup>6</sup>A antibody (Synaptic Systems; 212B11) at 1:1000 dilution was applied for 2 hr incubation at room temperature. After 3 washes in PBST, the membrane was incubated in HRP-conjugated anti-mouse IgG secondary antibody for 2 hr at room temperature, then washed again 3 times in PBST. Finally, the signal was visualized using SuperSignal West Dura Extended Duration Substrate (Thermo Scientific; 34075). To confirm equal mRNA loading, the same membrane was stained with 0.02% methylene blue in 0.3 M sodium acetate (pH 5.2). Quantified m<sup>6</sup>A levels were normalized to the amount of mRNA loaded.

### Immunohistology, imaging and analysis

Immunohistology was performed as described previously (Weng et al., 2017). Briefly, samples were collected from perfused animals, post-fixed overnight in 4% PFA in PBS, and cryoprotected in 30% sucrose (wt/vol) for 24 hr at 4°C. Samples were sectioned to 20  $\mu$ m and mounted onto slides. Primary antibody was applied at 4°C overnight. Secondary antibody was applied for 2 hr at room temperature. The following primary antibodies were used in this study: rabbit anti-m<sup>6</sup>A (Synaptic Systems; 212B11; 1:2000), rabbit anti-ATF3 (Santa Cruz; sc-188; 1:500), rabbit anti-PGP9.5 (AbD Serotec; 7863-0504; 1:800), rabbit anti-SCG10 (Novus Biologicals; NBP1-49461, 1: 2000), and anti-cleaved (active) form of caspase 3 (Invitrogen; 9H19L2; 1:500). Secondary antibodies corresponding to the primary antibody species were Cy2-, Cy3- or Cy5 conjugated (Jackson ImmunoResearch; 1:500). The images were acquired by confocal microscopy (Zeiss 710) and analyzed with ImageJ software (National Institutes of Health).

Quantification of the proportion of ATF3<sup>+</sup> neurons was determined by counting and scoring at least 200 neurons/mouse as ATF3<sup>+</sup> or ATF3<sup>-</sup> (Weng et al., 2017). A cell was scored as ATF3<sup>+</sup> if there was any fluorescence above the threshold set in ATF3<sup>-</sup> cells under the naive conditions. Sections were randomly chosen from cross-sectioned L4/L5 DRGs.

### Measurement of newly synthesized protein

WT and *Syn1-Cre;Mettl14<sup>fl/fl</sup>* (cKO) mice at 8-10 weeks of age were injected with puromycin (10 mg/kg, intraperitoneal, i.p.) at SNL D1. After 1 hr labeling, L4/L5 naive or injured DRGs were collected and processed for western blot as previously described (Weng et al., 2017). Briefly, protein samples were separated by 10% Mini-PROTEAN TGX Precast Protein Gels (Bio-rad) and transferred to PVDF membrane using the transblot turbo system (Biorad) following manufacturer's instructions. The membrane was incubated in blocking buffer (5% non-fat dry milk and 0.1% Tween 20 in TBS) for 1 hr at room temperature and then in mouse anti-puromycin antibody (MABE343; Millipore; 1:1000) at 4°C overnight. The blots were washed and incubated in HRP-conjugated goat anti-mouse IgG (Santa Cruz; sc-2031; 1:5000) at room temperature for 1 hr. Membranes were stripped and re-blotted with rabbit anti-GAPDH antibodies (Abcam; ab9485; 1:2000) as the loading control. Newly synthesized protein was quantified by measuring signal intensities at different size ranges from 198 to 15 KDa. Signals were quantified using ImageJ and data were normalized to that of the WT naive conditions in the same blots.

### Capillary electrophoresis immunoassay

The time course of the expression of ATF3 protein was determined by the capillary electrophoresis immunoassay using the Simple Western system as described previously. In brief, L4/L5 naive or injured DRGs were collected 1, 3, and 7 days post-SNL. Tissues were homogenized in CellLytic M (Sigma; C2978) containing a protease inhibitor cocktail (Sigma; 4693159001). The lysate protein concentration was determined using the Pierce BCA protein assay kit (Thermo Scientific; 23227). Equal amounts of DRG lysates (1  $\mu$ g) were mixed with Simple Western reagents and loaded to each capillary. The primary antibodies were diluted with antibody diluent (ProteinSimple) at 1:50 for anti-ATF3 (Santa Cruz; sc-188), 1:50 for anti-Mettl14 (Proteintech; 26158-1-AP), and 1:50 for anti-GAPDH (Abcam; ab9485).

### Western blot analysis

L4/L5 injured or naive DRGs were rapidly dissected and extracted protein samples were run on 10% Mini-PROTEAN TGX Precast Protein Gels (Bio-rad) and transferred to PVDF membrane. The membrane was blocked overnight in 5% dry milk at 4°C with rocking. Rabbit anti-YTHDF1 antibody (Proteintech; 1:1000) was applied overnight at 4°C followed by HRP-conjugated anti-rabbit IgG antibody (Santa Cruz; 1:10000). Protein loading was verified by mouse anti-GAPDH (EMD Millipore; AB2302).

### In vivo DRG axon regeneration assay

To measure regeneration of the sciatic nerve, samples were collected at SNL D3 and prepared as described above. Samples were sectioned longitudinally at 30  $\mu$ m and stained with SCG10 (Novus Biologicals, NBP1-49461). An SCG10 intensity plot was created using average intensities calculated across 10  $\mu$ m non-overlapping regions and normalized. Intensity was measured by ImageJ as previously described (Di Maio et al., 2011; Shin et al., 2012; Weng et al., 2017)

Punch biopsies of glabrous footpad skin from hind paws were collected for the quantification of nerve re-innervation (see Figure S2J in Weng et al., 2017). The biopsy was prepared and post-fixed in Zamboni's fixative. Samples were mounted on gelatin-coated slides and stained with rabbit anti-PGP9.5 which visualizes nerve fibers. To quantify regeneration, nerve fiber density was counted across 3 zones (defined in Figure 2F in Weng et al., 2017).

### Behavioral analysis

The thermal withdrawal behavioral test was performed following a previously established protocol (Wright et al., 2014). Briefly, the mice were placed on a glass surface with a consistent temperature of 30°C. The plantar surface of the hindpaw was heated using a focused, radiant heat light source (model 33 Analgesia Meter; IITC/Life Science Instruments, Woodland Hills, CA, USA). A timer linked to the light source was used to measure the paw-withdrawal latency. Only quick hind paw movements away from the stimulus were considered to be a withdrawal response, and seven individual measurements were repeated for each paw (Weng et al., 2017).

### Optic nerve regeneration quantifications

Quantification was performed as previously described (Park et al., 2008). For RGC regenerating axon quantification, the number of axons at different distances from the injury site was estimated by the following formula:  $\sum ad = \pi r^2 \times$  [average axon numbers per mm/t], where  $r$  is equal to half the width of the nerve at the counting site, the average number of axons per millimeter is equal to the average of (axon number)/(nerve width) in four sections of one optic nerve, and  $t$  is equal to the section thickness (8  $\mu\text{m}$ ). For RGC survival and pS6<sup>+</sup> RGCs quantification in the whole mount retina preparation, twelve images (three from each quarter, covering from inner to outer retina) of each retina were captured under a confocal microscope. Tuj1<sup>+</sup> or pS6<sup>+</sup> RGCs were quantified in a blinded fashion. Quantification of SMI32<sup>+</sup> RGCs was performed from images of Tuj1 and SMI32 immunostaining on retina sections.

## QUANTIFICATION AND STATISTICAL ANALYSIS

Data in figure panels reflect several independent experiments performed on different days.

The number of animals used for experiments is listed in the figure legends. An estimate of variation within each group of data is indicated using standard error of the mean (SEM). We performed two-way ANOVA tests for assessing the significance of differences between two treatments based the data properties or as indicated in the figure legends.

## DATA AND SOFTWARE AVAILABILITY

The accession number for the data for m<sup>6</sup>A-SMART-seq, m<sup>6</sup>A-SMART-CLIP-seq, and RNA-seq reported in this study is GEO: GSE106423.